The DRY Motif as a Molecular Switch of the Human Oxytocin Receptor†

Nicolas Favre,‡ Francesca Fanelli,*,§ Marc Missotten,‡ Anthony Nichols,‡ Janet Wilson,‡ Mariastella di Tiani,‡ Christian Rommel,‡ and Alexander Scheer*,‡

Serono Pharmaceutical Research Institute, 14, Ch. des Aulx, 1228 Plan-les-Ouates, Geneva, Switzerland, and Dulbecco Telethon Institute and Department of Chemistry, University of Modena and Reggio Emilia, 41100 Modena, Italy

Received May 26, 2005

ABSTRACT: The human oxytocin receptor is known to exhibit promiscuous activity by coupling to both $G\alpha_q$ and $G\alpha_i$ G proteins to activate distinct signaling pathways. A single-amino acid substitution within the highly conserved E/DRY motif at the cytosolic extension of helix 3 [i.e., D136(3.49)N] increased the rate of both basal and agonist-stimulated inositol phosphate (IP_3) accumulation of the receptor. Furthermore, like for a typical constitutively active receptor, the partial agonist arginine vasopressin behaved as a full agonist for the D136(3.49)N mutant. Subsequently, both oxytocin and arginine vasopressin showed an increased potency in stimulating IP3 accumulation as compared to the wild-type receptor. Very interestingly, our experiments provide strong evidence that the D136(3.49)N mutant inhibits receptor signaling via $G\alpha_i$-mediated pathways while increasing the activity through the $G\alpha_q$-mediated pathways. Molecular simulations of the free and OT-bound forms of wild-type OTR and of the D136(3.49)N constitutively active mutant suggest that the receptor portions close to the E/DRY and NPxxY motifs are particularly susceptible to undergoing structural modification in response to activating mutations and agonist binding. Furthermore, computational modeling suggests that the OT-bound form of wild-type OTR is able to explore more states than the OT-bound form of the D136(3.49)N constitutively active mutant, consistent with its G protein promiscuity. Taken together, these observations emphasize the important role of the E/DRY motif not only in receptor activation but also in the promiscuity of G protein coupling. Knowledge of the mechanism of selective G protein coupling could aid drug discovery efforts to identify signaling specific therapies.

G protein-coupled receptors (GPCRs)[1] represent the largest family of cell surface receptors known and are structurally characterized by seven transmembrane (TM) α-helices connected by alternating extracellular and intracellular loops (EL and IL, respectively) (*1*−*3*). Mutational analysis has revealed that the extracellular halves of these receptors are primarily involved in ligand binding, whereas the cytosolic loops mediate the interaction with one or more heterotrimeric G proteins to trigger intracellular signaling (*1*−*3*). In many cases, ligands bind within the core of the helix bundle forming multiple connections with amino acid residues located in different domains, including both helices and loops as often observed for peptide receptors. Sometimes, the binding site is entirely located on a large and highly structured amino-terminal domain, as for amino acids or glycoprotein hormone receptors (*1*−*3*).

Mammalian GPCRs tend to fall into one of three families termed A, B, and C (*2*, *3*). Family A is the rhodopsin-like or adrenergic receptor-like family; family B is the glucagon receptor-like or secretin receptor-like family, and family C is the metabotropic glutamate neurotransmitter receptor family (*1*−*3*).

An increasing number of GPCRs are found to be promiscuous in that they can couple to more than one G protein to activate multiple signaling pathways (*4*−*7*). No obvious sequence homology was observed even for GPCRs that coupled to the same G protein subtype, and no consensus motif predicative of G protein coupling specificity has been identified to date (*8*). However, a growing number of mutagenesis (*9*−*12*) and theoretical (*13*−*15*) studies have suggested that the cytosolic extensions of helices 3 and 6 as well as IL2 and -3 of some GPCRs can determine the efficiency and selectivity of receptor−G protein coupling. More specifically, the DRY motif is a highly conserved triplet of amino acids, located at the cytosolic extension of helix 3 of GPCRs of the rhodopsin family (*2*, *3*, *16*) and implicated to play a pivotal role in constitutive (agonist-

† This study was supported by Telethon-Italy Grant TCP00068 and by the Compagnia S. Paolo (Grant TCP00068.CSP01) (to F.F.).

* To whom correspondence should be addressed. A.S.: Department of Molecular Screening and Cellular Pharmacology, Serono Pharmaceutical Research Institute, Ch. des Aulx 14, 1228 Plan-les-Ouates, Geneva, Switzerland; telephone, 004122-706-98-36; e-mail, alexander.scheer@serono.com. F.F.: Dulbecco Telethon Institute and Department of Chemistry, University of Modena and Reggio Emilia, Via Campi 183, 41100 Modena, Italy; telephone, +39-059-2055114; e-mail, fanelli@unimo.it.

‡ Serono Pharmaceutical Research Institute.

§ University of Modena and Reggio Emilia.

[1] Abbreviations: GPCR, G protein-coupled receptor; OTR, oxytocin receptor; OT, oxytocin; AVP, arginine vasopressin; GTPγS, guanosine (3′-*O*-thio)triphosphate; PTX, pertussis toxin; PI-PLC, phosphoinositol specific phospholipase C; IP3, inositol 1,4,5-triphosphate; DAG, 1,2-diacylglycerol; PKC, protein kinase C; MAPK, mitogen-activated protein kinase; GEF, guanosine nucleotide exchange factor; MEK, MAPK/ERK kinase; ERK, extracellular signal-regulated kinase; OVTA, ornithine vasotocin analogue; AKT, protein kinase B; SPA, scintillation proximity assay; LHR, luteinizing hormone receptor; AR, adrenergic receptor; HTR, serotonin receptor.

10.1021/bi0509853 CCC: $30.25
Published on Web 07/08/2005

independent) receptor activation and signal transduction pathways (*17*−*26*). The arginine residue is fully conserved, and mutagenesis studies have suggested that it is essential for constraining the receptor in an inactive state (*19*−*21*). The adjacent aspartate residue is also highly conserved and plays an important role in receptor activation as mutations of this residue are reported to result in constitutive activation of some GPCRs, including rhodopsin (*22*), and the α_{1b} adrenergic (*17*, *18*), β_2 adrenergic (*23*), histamine H_2 (*24*), vasopressin V2 (*25*), and muscarinic M_1 (*26*) receptors.

The OT receptor (OTR) is one receptor that demonstrates promiscuous G protein coupling for which no conclusive evidence regarding the role of the DRY motif on constitutive activity and G protein coupling promiscuity has been reported to date. The OTR belongs to family A (rhodopsin-like) of GPCRs and share a high degree of sequence similarity to arginine vasopressin (AVP) receptor subfamily members V_{1a}, V_{1b}, and V_2. The hormone OT is a nine-amino acid peptide (Cys-Tyr-Ile-Gln-Asn-Cys-Pro-Arg-Gly-NH_2) and acts as a potent uterotonic agent to play an important role in parturition and lactation via an action on myometrial OTRs. Immediately before parturition, OTRs show a dramatic increase in their levels of expression, which could induce preterm labor by sensitizing the uterus to the relatively unchanged circulating levels of OT (*27*, *28*). Clinically, OT is administered to induce labor, whereas OT antagonists could provide a unique approach for the prevention of preterm labor by prolonging uterine quiescence (*29*−*32*).

The OTR is coupled to both PTX sensitive $G\alpha_i$ and insensitive $G\alpha_q$ G proteins, which subsequently activate at least two major different signaling pathways (*33*, *34*). Activation of $G\alpha_q$ pathways stimulates phospholipase C (PLC), leading to an increased level of hydrolysis of phosphatidylinositol 4,5-biphosphate to inositol 1,4,5-triphosphate (IP_3) and 1,2-diacylglycerol (DAG) which increase intracellular Ca^{2+} concentrations and activate protein kinase C (PKC), respectively. Subsequently, PKC activates the mitogen-activated protein kinase (MAPK) cascade, a vital signaling pathway component in an increasing number of hormonally responsive cells (*35*). In addition, the ability of the OTR to activate $G\alpha_i$ recruits the adaptor protein Grb2 in a complex with the guanosine nucleotide exchange factor (GEF) Sos. However, for a full mitogenic response to occur, active Ras-GTP must couple to various effector pathways such as the Ser/Thr kinase c-Raf. Once activated, Raf phosphorylates the MAPK/ERK kinase (MEK), which in turn phosphorylates and activates the p42 and p44 MAPKs (ERK1/2).

Very little is known about structure−function relationships related to G protein coupling specificity in the OT/vasopressin receptor subfamily. Mutagenesis studies revealed that all of the intracellular domains of the OTR contained determinants that influenced $G\alpha_q$-mediated coupling to PLC (*36*) with K270(6.30) [the amino acid numbering in parentheses, used only for the amino acids in the helix bundle, is that proposed by Ballesteros and Weinstein (*37*)],[2] in the cytosolic extension of helix 6, playing an essential role (*38*). Additional evidence also indicated that the proximal 51 amino acids of the COOH terminus were required for coupling to $G\alpha_q$, but not for the $G\alpha_i$-mediated signaling pathways (*34*).

This study is based on the integration between in vitro experiments and computational modeling. In vitro experiments were essentially aimed at finding novel constitutively active OTR mutants and at investigating further the OTR features, which regulate coupling to $G\alpha_q$ and $G\alpha_i$ proteins. Computational modeling was aimed at inferring the structural features differentiating the nonactive from the active forms of OTR as well as those features which make the difference between OT-bound forms of WT OTR and OT-bound forms of the D136(3.49)N constitutively active mutant discovered in this work.

Taken together, our studies suggest that the DRY motif, besides playing a crucial role in receptor activation, may also be implicated in receptor promiscuity.

MATERIALS AND METHODS

Materials. COS-7 cells and HEK/EBNA cells were obtained from American Type Culture Collection (Rockville, MD) or Invitrogen (Carlsbad, CA), while Dulbecco's Modified Eagle's Medium (DMEM), L-glutamine, penicillin/streptomycin, and fetal bovine serum (FBS) were purchased from GibcoBRL (Basel, Switzerland). The Vent DNA polymerase, restriction enzymes (EcoRI and SalI), and T_4 DNA ligase were purchased from BioLabs (Beverly, MA). The pRK5 expression vector and the human OTR gene were generous gifts from S. Cotecchia (Institute of Pharmacology, Lausanne, Switzerland) and C. Barberis (INSERM, Montpellier, France), respectively. Radioactive inositol, myo[2-^{3}H(N),^{125}I]ornithine vasotocin analogue (OVTA), and [*tyrosol*-2.6-^{3}H]oxytocin were purchased from NEN (Boston, MA), and ligands AVP and OT were from BACHEM (Bubendorf, Switzerland). The phospho specific antibodies [P-AKT (Ser473) and P-ERK1/2] and the non-phospho specific antibodies (AKT and ERK) were purchased from Cell Signalling, while PI3K inhibitor LY294-002 was from Calbiochem (Basel, Switzerland). All other reagents were obtained from standard commercial sources.

Mutagenesis. The cDNA encoding human OTR was mutated by polymerase chain reaction (PCR)-mediated mutagenesis and Vent DNA polymerase. The mutated DNA fragments were assembled by PCR, digested for 2−3 h at 37 °C with EcoRI and SalI restriction enzymes, and subcloned into the pRK5 expression vector following an overnight incubation at 15 °C with T_4 DNA ligase. The new construct was transformed in DH10β competent cells by electroporation; colonies were isolated in ampicillin dishes after an overnight incubation at 37 °C, and sequences were confirmed by automated DNA sequencing (ABI Prism 3700 DNA Analyzer).

Cell Culture and Transient Expression. COS-7 cells were grown in DMEM supplemented with 10% FBS, 2 mM L-glutamine, and penicillin/streptomycin (20 μg/mL). The cells were transiently transfected with expression vectors harboring the WT (0.15−1 μg/10^6 cells) or mutant (0.75−3 μg/10^6 cells) receptors using the Fugene-6 method according to the manufacturer's instructions. Membrane preparations and IP_3 accumulation experiments were performed 42−48 h following transfection.

[2] According to the numbering system of Ballesteros and Weinstein (*37*), every amino acid identifier starts with the helix number, followed by the position relative to a reference residue among the most conserved amino acids in that helix. That reference residue is arbitrarily assigned the number 50.

HEK/EBNA cells were grown and transfected in the same medium and cultured under the same conditions as the COS-7 cells.

Measurements of IP_3. Transfected COS-7 or HEK/EBNA cells (7.5×10^5 cells) were seeded in a 12-well plate and labeled for 17 h with [2-^{3}H(N)]myoinositol at 4 μCi/mL in inositol-free DMEM supplemented with 1% FBS. Cells were preincubated for 10 min in PBS containing LIL (20 mM) and stimulated with OT or AVP for 30−45 min. The reaction was stopped with perchloric acid (0.4 M) and the mixture neutralized with KOH and $KHCO_3$. Total IPs were extracted and separated using a strong anion exchange column (AG 1-X8, formate form; 100−200 mesh; Bio-Rad). Following two wash steps with water, the columns were eluted with an elution solution containing ammonium formate (1 M) in formic acid (25.9 M). At each concentration, a fraction containing inositol monophospates, biphosphates, and triphosphates was collected, and radioactive IP levels were determined by means of liquid scintillation counting using a Beckman LS6000TA reader. This fraction is termed total IPs and expressed as disintegrations per minute per well.

Membrane Preparation and Radioligand Binding. Transfected cells were washed twice with ice-cold phosphate-buffered saline (PBS), scraped in a lysis buffer [10 mM $MgCl_2$, 2 mM EDTA, and 50 mM Tris (pH 7.5)], and homogenized in a glass potter (20−30 strokes). Following an initial centrifugation step (500−1000 rpm or 250*g* for 5 min), a second ultracentrifugation step (18 000 rpm or 145000*g* for 40−60 min at 4 °C) was used to pellet the membranes. These membranes were resuspended in binding buffer [10 mM $MgCl_2$, 10 mM HEPES (pH 7.4), and 0.1% BSA (pH 7.5)] and used immediately or stored at −80 °C.

For the scintillation proximity assays (SPAs), 5−15 μg of membranes was incubated with 0.1 nM [^{125}I]OVTA, agonist, and PVT PEI-treated beads (100 μg/well) in a total assay volume of 100 μL. Nonspecific binding was assessed in the presence of OT (1 μM). The reaction mixture was incubated for 1 h at room temperature and then read in a Wallac Trilux 1450 Microbeta counter (Perkin-Elmer).

For filtration binding assays, 50 μg of membranes was incubated with 1.1 nM [^{3}H]oxytocin and agonist in a total assay volume of 200 μL. Nonspecific binding was assessed in the presence of OT (1 μM). The reaction mixture was allowed to incubate for 2 h at room temperature. Unifilter350 GF/C plates (Whatman) were used and pretreated with 0.5% PEI (polyethyleneimine). Three washes of 10 s were performed before the plates were dried at 40 °C for 1 h; 100 μL of scintillation liquid was added, and the plates were read in a Wallac Trilux 1450 Microbeta counter (Perkin-Elmer).

For the competition binding experiments, PTX was added (200 ng/mL) to the medium 24 h before the membrane preparation. For the GTPγS experiments, the membranes were preincubated with 100 μM GTPγS at 4 °C for 30 min. For competition experiments, in SPA, 0.3 nM [^{125}I]OVTA was used in competition with an increasing concentration of cold OT (from 1 pM to 100 μM). For the filtration competition binding experiments, a concentration of 1.2 nM [^{3}H]oxytocin was used in competition with an increasing concentration of cold OT (from 1 pM to 100 μM). For competition assays, filtration, or SPA, other conditions are similar to those of the binding assays previously described.

Data Analysis. Data were analyzed with Prism (GraphPad Software Inc., San Diego, CA). K_i values were calculated from IC_{50} values using the Cheng−Prusoff equation (*39*).

Western Blot Analysis. HEK/EBNA cells stably expressing the human WT or mutant OTR or HEK/EBNA cells transiently transfected with the human WT or mutant OTR were seeded (2×10^6 cells/well) in 10 cm plates in serum-free medium. Forty-eight hours following transfection, cells were stimulated for 5 min with OT (200 nM) and lysed in a detergent RIPA buffer [50 mM Tris-HCl (pH 7.5), 0.5% Triton X-100, 3 mM EGTA, 12 mM β-glycerophosphate, 150 mM NaCl, 50 mM NaF, 1 mM sodium vanadate, 2 mM DTT, and 1 mM phenylmethanesulfonyl fluoride]. The cell lysate was then centrifugated at 13000*g* for 10 min at 4 °C. The resulting supernatants were diluted (1:5) in SDS sample buffer, electrophoresed on a 10% acrylamide gel and transblotted onto a nitrocellulose membrane. After being blocked with TBS, 0.1% Tween, and 5% BSA, the membranes were incubated overnight at 4 °C with antibodies to either P-Akt (Ser473) or P-ERK1/2 (1:1000). The membranes were then washed extensively with TBS and 0.1% Tween, and detection using a secondary antibody was performed using standard protocols with peroxidase-coupled antisera and enhanced chemiluminescence (ECL Western Blotting Detection Reagents, Amersham Biosciences).

Comparative Modeling of the OTR and MD Simulations. A new model of the human OTR was built by comparative modeling [i.e., through MODELER (*40*)], by using the 2.8 Å X-ray crystal structure of rhodopsin as a template (*41*). The model of OTR lacks the last 42 amino acids.

Different chimeric rhodopsin−OTR templates were probed. In the final chimeric template, helices 5 and 6 were prolonged at their cytosolic ends by 10 and 6 amino acids from the OTR sequence, respectively, after deletion of stretches of rhodopsin residues 225−235 and 240−248, respectively (i.e., bold characters in the rhodopsin sequence in Figure 1). Furthermore, such helices were connected by a model of IL3, based upon the results of fold recognition (i.e., bold characters in the rhodopsin sequence in Figure 1). Moreover, the C-tail of rhodopsin was truncated at C223. Slightly different sequence alignments were probed. The OTR model presented in this work was produced by means of the alignment shown in Figure 1. Since, according to such alignment, a four-amino acid insertion occurs in the N-terminal half of helix 1 of the OTR (Figure 1), α-helical restraints were imposed to the stretch of amino acids 32−47, during comparative modeling. For each of the different input templates and/or alignments, MODELLER generated 50 models, by randomizing the Cartesian coordinates of the model through a random number uniformly distributed in an interval from −4 to 4 Å (*40*). Among the 450 models finally obtained, 10 models were selected, which showed low restraint violations associated with high values of the 3D-Profile score, computed by means of the Protein Health module in the QUANTA 2000 package (www.accelrys.com), and low numbers of main chains and side chains in nonallowed conformation and close contacts. These models were first completed by the addition of the polar hydrogens and then subjected to automatic and manual rotation of the side chain torsion angles when in nonallowed conformations as well as to in vacuo energy minimization and MD simulations by means of the charmm program (*42*). Mini-

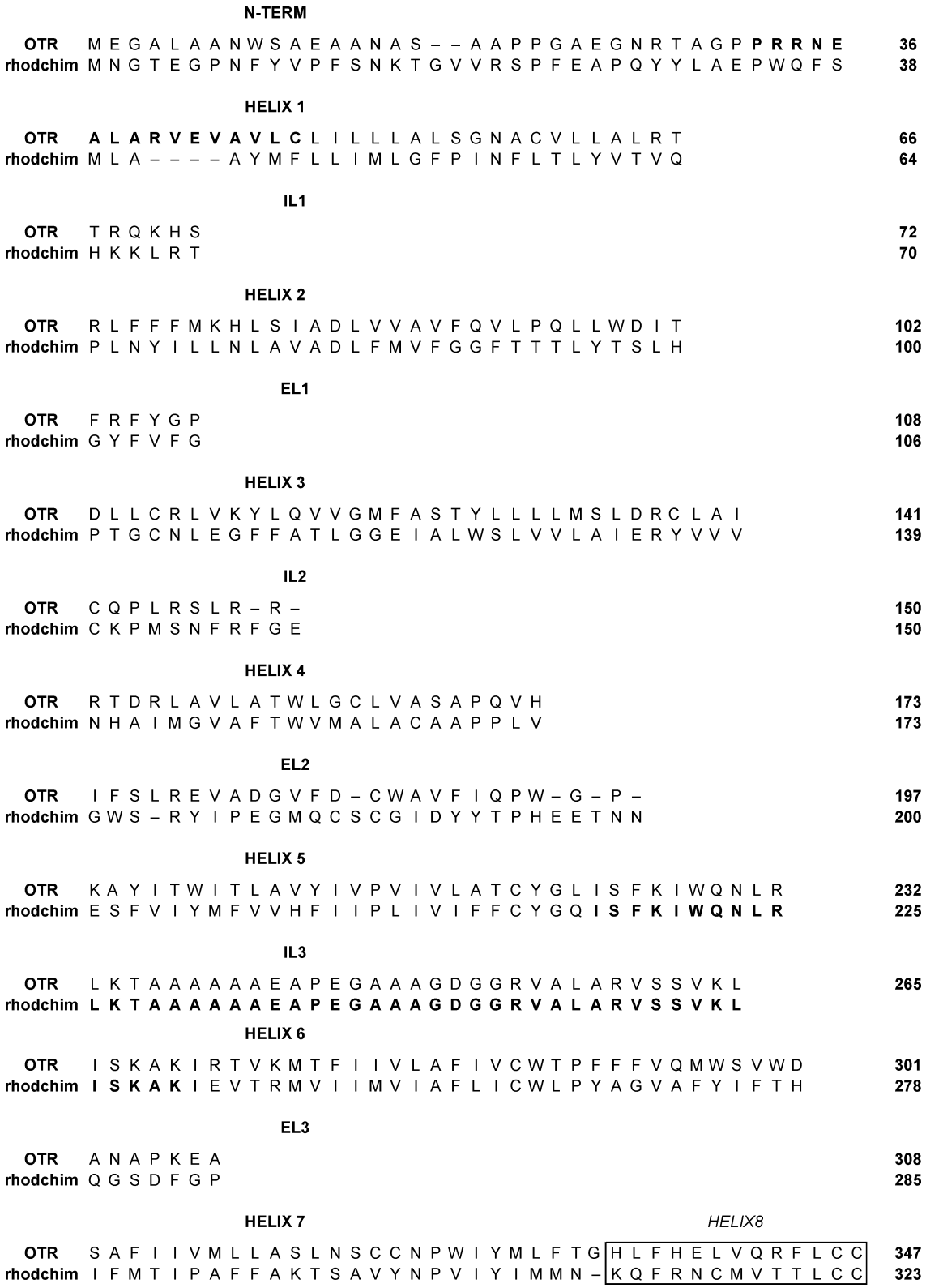

FIGURE 1: Sequence alignment of a rhodopsin chimeric template (rhodchim) and the human OTR. In detail, the rhodopsin structure has been subjected to deletions of the following amino acid segments: residues 225−235 and 240−248 (both from I3) followed by the addition of the amino acid segment of residues 223−271 representing the cytosolic extensions of helices 5 and 6 and IL3 of OTR (bold characters on the rhodopsin sequence). The OTR sequence of residues 32−47, corresponding to the extracellular half of helix 1, was subjected to α-helical restraints during comparative modeling (i.e., bold characters). The amino acids, which belong to "helix 8", at the cytosolic extension of helix 7, are boxed, both in OTR and in rhodopsin sequences.

mizations were carried out by using 1500 steps of steepest descent followed by a conjugate gradient minimization, until the root-mean-square gradient was less than 0.001 kcal mol^{-1} Å. A distance-dependent dielectric term ($\epsilon = 4r$) was chosen. The "united atom approximation" was used for the receptor protein. MD simulations were carried out on the minimized coordinates of WT and mutated OTR in their free and ligand-bound forms. The lengths of the bonds involving the

hydrogen atoms were restrained according to the SHAKE algorithm, allowing an integration time step of 0.001 ps. The systems were heated to 300 K with a 5 K increase, every 100 steps per 6000 steps, by randomly assigning velocities from the Gaussian distribution. After heating, the system was allowed to equilibrate for 34 ps. A disulfide bridge patch was applied to C112(3.25) and C187 in EL2 as well as to Cys1 and Cys6 of the peptide OT (the one-letter code is employed for the amino acids in the receptor, whereas the three-letter code is employed for the amino acids which constitute the hormone).

The secondary structure of the helix bundle was preserved, by assigning distance restraints (i.e., minimum and maximum allowed distances of 2.7 and 3.0 Å, respectively) between the backbone oxygen atom of residue i and the backbone nitrogen atom of residue $i + 4$. The scaling factor of such restraints was 10, and the force constant at 300 K was 10 kcal mol^{-1} Å. The application of these intrahelical distance restraints was instrumental in (a) reducing the system degrees of freedom, (b) inferring the structural and dynamic role of prolines, and (c) letting the helices move as rigid bodies, consistent with the experimental evidence for rhodopsin activation (*43*).

For the empty receptor forms, short (100 ps) equilibrated MD runs were carried out, probing different input structures and different combinations of intrahelical distance restraints. The latter tests consisted of applying distance restraints to different amino acid stretches in each helix. Finally, the computation conditions and the input receptor structure were chosen, which, following MD simulation, produced average arrangements characterized by a good quality (evaluated by means of the Protein Health module in the QUANTA 2000 package) together with structural similarity to rhodopsin. The similarity between the average minimized structures of the empty OTR and rhodopsin structure was evaluated on the basis of the root-mean-square deviation (rmsd) of the main chain backbone atoms in the transmembrane domains as well as the degree of conservation of the interaction patterns involving the conserved amino acids.

The finally selected intrahelical distance restraints involved the following amino acid stretches: (a) 32−66 in helix 1, (b) 73−102 in helix 2, (c) 109−141 in helix 3, (d) 152−173 in helix 4, (e) 199−232 in helix 5, (f) 267−301 in helix 6, (g) 311−332 in helix 7, and (h) 333−347 in "helix 8". The backbone oxygen atoms of the amino acids at position $i - 4$ with respect to prolines were not subjected to distance restraints. Furthermore, the backbone oxygen atoms of the amino acid stretches of residues 204−206 in helix 5 were subjected to distance restraints with the backbone nitrogen atoms at position $i + 5$. Finally, as for helix 7, the backbone oxygen atom of amino acid 316 was not subjected to restraints, whereas those in the stretch of residues 317−319 were subjected to distance restraints with the backbone nitrogen atoms at position $i + 3$. These conditions allowed us to better account for the irregularities in the α-helical conformation in the extracellular halves of helices 5 and 7, as inherited from rhodopsin structure. These conditions of intrahelical distance restraints were used also for relatively long (1 ns) MD simulations of the empty receptors.

The computation conditions and the input structure selected, based upon MD simulations of the empty WT OTR, were used for simulating all the other forms considered in this study.

The structure of OT employed for generating the OT−OTR complexes was the one extracted from the crystal structure of the OT−neurophysin complex [PDB entry 1npo (*44*)]. Furthermore, the carboxy function of Gly9 was substituted with an amide. Approximately 350 different input structures of the OT−OTR complexes were built by manual docking, taking into account the information from the experimental data on OTR and other GPCRs (*45*−*50*). This information and the results of quality checks on the average minimized structures of the OT−OTR complexes from the short MD trajectories were in turn used for selecting the trajectories, which would be worth prolonging to 1 ns.

Testing was carried out on the WT OTR carrying D136(3.49) in its unprotonated form. The selected input structures of the free OTR as well as of the OT−OTR complexes were used to build the free and OT-bound forms, respectively, of the D136(3.49)N constitutively active mutant. Such mutated forms of OTR were subjected to 1 ns MD simulations as well. Different allowed conformations of the N136(3.49) side chain were probed.

To provide more strength to the results of in vacuo computations, small variances of the selected input structures of the empty and bound forms of WT and mutated OTR were subjected to energy minimization and 1 ns MD simulations using an implicit membrane−water model (i.e., IMM1) recently implemented in charmm (*51*). This is an extension of the EEF1 implicit water salvation model to heterogeneous membrane−aqueous media (*51*). Different MD runs were carried out, probing different computation conditions. In the setup finally selected, the adjustable parameter "*a*" and the nonpolar core thickness were set equal to 0.85 and 32 Å, respectively. Minimizations were carried out by using 1500 steps of steepest descent followed by a conjugate gradient minimization, until the root-mean-square gradient was less than 0.001 kcal mol^{-1} Å. The "united atom approximation" was employed. The lengths of the bonds involving the hydrogen atoms were restrained according to the SHAKE algorithm, allowing an integration time step of 0.001 ps. Heating followed the same setup as in vacuo simulations, whereas the length of equilibration was set equal to 64 ps. No intrabackbone distance restraints were assigned. The selected input structures of empty and OT-bound forms of WT OTR were also simulated for 1 ns by setting D136(3.49) in its protonated form [i.e., D136(3.49)PROT]. Different conformations of the protonated D136(3.49) side chain were probed by MD.

The analysis of the results of computational experiments was essentially based upon the comparisons of the structures averaged over different time periods of MD simulations.

RESULTS

In Vitro Experiments. The in vitro search for novel constitutively active OTR mutants was based upon the homologies with other GPCRs belonging to family A. The majority of the activating mutations, which were considered, are located at the cytosolic extensions of helices 3 and 6, whereas only two are located in helices 1 and 2 (Table 1). In particular, (a) A53(1.46) in OTR is homologous to A373(1.46) in the lutropin receptor (LHR) and mutation to V

Table 1: Mutations Introduced into the Human OTR

mutated residue in the OTR	location of mutation	constitutively active receptor	homologous mutated residue	refs
A53(1.46)V	helix 1	LHR	A373(1.46)V	*52, 53*
M78(2.43)T	helix 2	LHR	M398(2.43)T	*52, 53*
D136(3.49)N/A/V	helix 3	rhodopsin family	D136(3.49)A	*22−26*
R137(3.50)A/K	helix 3	OTR	R137(3.50)A	*19*
C138(3.51)A	helix 3	α_{1b}-AR	Y144(3.51)A	*54*
K270(6.30)R	helix 6	rhodopsin family	K270(6.30)R	*52−57*
V274(6.34)E/K/I	helix 6	α_{1b}-AR	A293(6.34)E/K	*58*

activates the latter (*52*, *53*). (b) M78(2.43) in OTR is homologous to M398(2.43) in LHR, and mutation to T activates the latter (*52*, *53*). (c) D136(3.49), of the conserved E/DRY motif, has been found to be susceptible to activating mutations in several members of the rhodopsin family (*22*−*26*). (d) C138(3.51) in OTR is homologous to Y144(3.51) in the α_{1b}-adrenergic receptor (α_{1b}-AR), in which mutation of this conserved tyrosine to alanine was found to be activating (*54*). (e) K270(6.30) in OTR is homologous to a glutamate/aspartate, which is found in rhodopsin and in many members of the rhodopsin family and which induces constitutive activation when replaced with neutral or cationic amino acids (*52*−*57*). Finally, (f) V274(6.34) in OTR is homologous to A293(6.34) in the α_{1b}-AR, and mutations to either E or K activate the latter (*58*).

Following transient transfection into COS-7 cells, cell surface expression could not be detected for several of these mutated receptors [A53(1.46)V, M78(2.43)T, D136(3.49)A/V, and V274(6.34)E/K] which excluded any further analysis. Low levels of cell surface expression could be detected for four of the remaining mutated receptors [K270(6.30)R, V274(6.34)I, C138(3.51)A, and R137(3.50)A], but when tested in a functional assay, OT-stimulated IP accumulation was impaired compared with the WT control (data not shown). Surprisingly, these nonexpressing receptors included the R137(3.50)A mutant, which was previously reported to show an enhanced basal level of IP3 production compared with that of the WT OTR (*19*).

Consistent with the results of mutagenesis experiments on other GPCRs (*17*−*19*, *22*−*26*), a mutation of the aspartate of the DRY motif induced constitutive activity to the OTR. We observed that, unlike with the D136(3.49)A and D136(3.49)V mutants, a D136(3.49)N mutant demonstrated a significantly increased (approximately 50%) basal level of IP3 accumulation compared with the WT receptor in COS-7 cells (Figure 2A) and HEK/EBNA cells (Figure 2B). As with basal levels, 10 μM OT was able to stimulate significantly more IP accumulation in D136(3.49)N-expressing cells compared with WT receptors [approximately 50% in COS-7 cells (Figure 2A) and 35% in HEK/EBNA cells (Figure 2B)]. The increased activity of D136(3.49)N was not simply due to a larger number of receptors expressed per cell since the expression level of D136(3.49)N was approximately half that of the WT receptor as shown with saturation binding experiments. Binding of [^{3}H]OT to both WT and D136(3.49)N receptors was saturable and of high affinity with calculated K_D values of 1.5 ± 0.5 and 1.3 ± 0.7 nM for WT and D136(3.49)N receptors, respectively (Table 2). However, D136(3.49)N receptors were expressed at a significantly lower level compared with the WT, with B_{max} values of 1000 ± 200 and 450 ± 100 pmol/mg, respectively ($n = 3$). Hence, our D136(3.49) mutant demonstrated higher basal and OT-stimulated IPs levels than the WT receptor, consistent with properties of a typical constitutively active receptor. Transient transfection of HEK/EBNA cells with the WT or mutant D136(3.49)N receptor yielded similar expression levels for both receptors (Table 2). Nevertheless, as observed in COS-7 cells, the D136(3.49)N mutant receptor exhibited a significantly higher level of basal IP3 accumulation than the WT receptor (Figure 2A).

Another common feature of constitutively active receptors is an increased potency for an agonist in a functional assay. This was investigated by comparing efficacy and potency values for WT and D136(3.49)N receptors for the full agonist OT and the partial agonist AVP in an IP3 accumulation

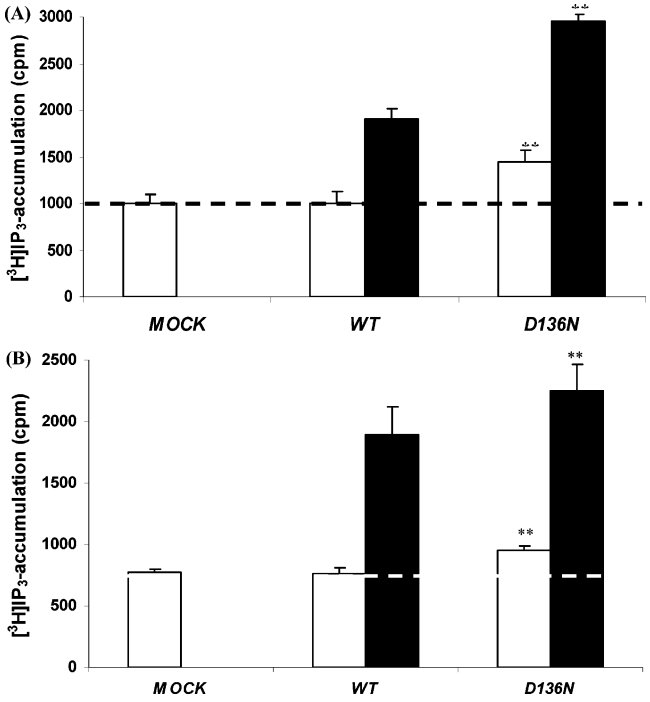

FIGURE 2: Basal and OT-stimulated IP_3 accumulation of the WT (□) and D136N OTR (■). WT and D136N receptors were transiently transfected in COS-7 (A) and HEK/EBNA (B) cells, and the accumulation of total IP_3 was assessed. The mean of five different experiments is shown; each experiment was performed in triplicate. The IP_3 production of the WT and D136N mutant was expressed in counts per minute. The expression level for the WT ($B_{max} = 700$ pmol/mg) was 2 times higher than the expression level of the D136N receptor ($B_{max} = 300$ pmol/mg). Cells were stimulated for 40 min in the absence or presence of 10 μM OT. The level of basal IP_3 accumulation of the D136N mutant was increased by 50% as compared with that of the WT. Data are given as the mean ± the standard error of the mean for three or more experiments; each experiment was performed in triplicate. Two asterisks indicate $p < 0.01$.

Table 2: K_D and B_{max} Values of the WT and Mutant D136(3.49)N OTR Measured by a [^{3}H]OT Filtration Assay in Transiently Transfected COS-7 and HEK/EBNA Cells

	COS-7		HEK/EBNA	
[^{3}H]OT[a]	B_{max} (fmol/mg)	K_D (nM)	B_{max} (fmol/mg)	K_D (nM)
WT OTR	1000 ± 200	1.5 ± 0.5	1700 ± 250	0.8 ± 0.1
D136N OTR	450 ± 100	1.5 ± 0.7	2450 ± 410	1.0 ± 0.2

[a] WT and D136(3.49)N were transiently transfected in COS-7 and HEK/EBNA cells, and the expression level using [^{3}H]OT was determined. The mean of three different experiments is shown; each experiment was performed in triplicate. A DNA ratio of 10:1 (D136N:WT OTR) was used for the transfection.

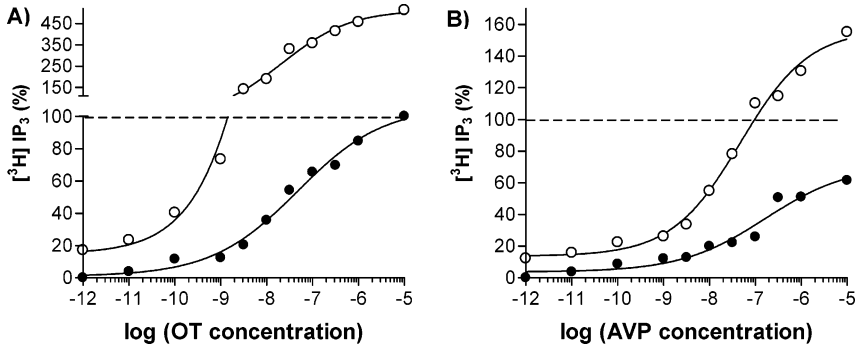

FIGURE 3: Comparison of agonist potencies at the WT (●) and D136N OTR (○). WT and D136N receptors were transiently transfected in COS-7 cells. Following stimulation for 40 min, the IP_3 accumulation was assessed in the presence of increasing concentrations of either oxytocin (OT) (A) or arginine vasopressin (AVP) (B). This is a schematic representation of three different experiments; each experiment was performed in triplicate.

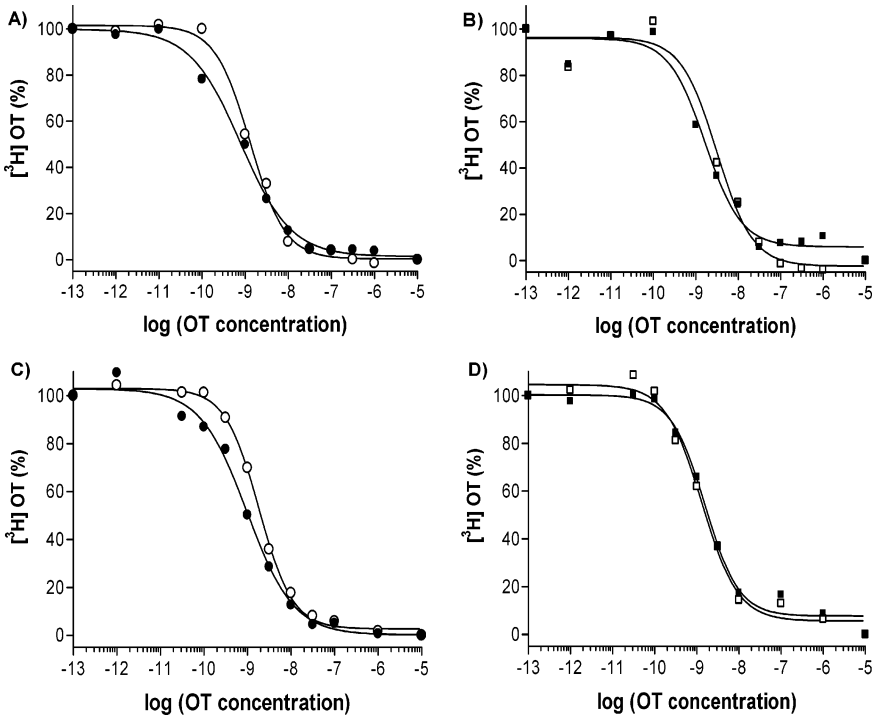

FIGURE 4: Competition binding of the WT and D136N OTR in the absence [WT (●) and D136N (■)] or presence [WT (○) and D136N (□)] of guanosine (3′-*O*-thio)triphosphate (GTPγS) or following treatment with pertussis toxin (PTX). Membranes were prepared from COS-7 cells transiently transfected with cDNA encoding either for the WT OTR (A−C) or for the D136N OTR (B−D). Competition binding using [^{3}H]OT was performed in the presence or absence of 100 μM GTPγS (A and B) or following 200 ng/mL PTX (C and D). Data are given as the mean ± the standard error of the mean for three or more experiments; each experiment was performed in triplicate.

assay. As shown in Figure 3A, increasing concentrations of OT dose-dependently increased the level of IP3 accumulation at both WT and D136(3.49)N receptors. However, the potency of OT was significantly higher ($p < 0.05$) in D136-(3.49)N than in WT cells (EC_{50} of 22 ± 5 and 47 ± 10 nM, respectively). Furthermore, the D136(3.49)N receptors had an increased efficacy, with maximum IPs levels accumulated being 385% times that of the WT receptor. Similarly, using the partial agonist AVP, potency and efficacy values were increased with the D136(3.49)N mutant (EC_{50} of 47 ± 6 and 166 ± 21 nM, respectively). As we previously observed in Figure 2, basal IP3 levels were higher in the D136(3.49)N receptor than in the WT (Figure 3A,B).

To further characterize the pharmacology of the mutated D136(3.49)N receptor, K_i values for OT were determined in homologous competition binding experiments using [^{3}H]-OT. For the WT receptor, competition curves were characterized by Hill coefficients of less that unity and data were best-fitted to a two-site binding model, revealing high (K_h) and low (K_l) dissociation constants of 1.6 ± 0.2 and 16 ± 6 nM, respectively (Figure 4A). In contrast, the displacement curve for OT at the D136(3.49)N mutant receptor was monophasic, with a Hill coefficient of unity and a K_l value of 12 ± 1 nM (Figure 4B).

To further investigate this phenomenon, we performed competition binding experiments on WT and mutant receptors in the presence of 100 μM GTPγS, a nonhydrolyzable analogue of GTP that disrupts the interaction of receptors with G proteins. In the presence of GTPγS, binding data were best described by a one-site binding model, with a K_i value of 1.3 ± 0.3 nM (Figure 4A). In contrast, no changes were observed at the D136(3.49)N receptor (K_i = 3.15 ±

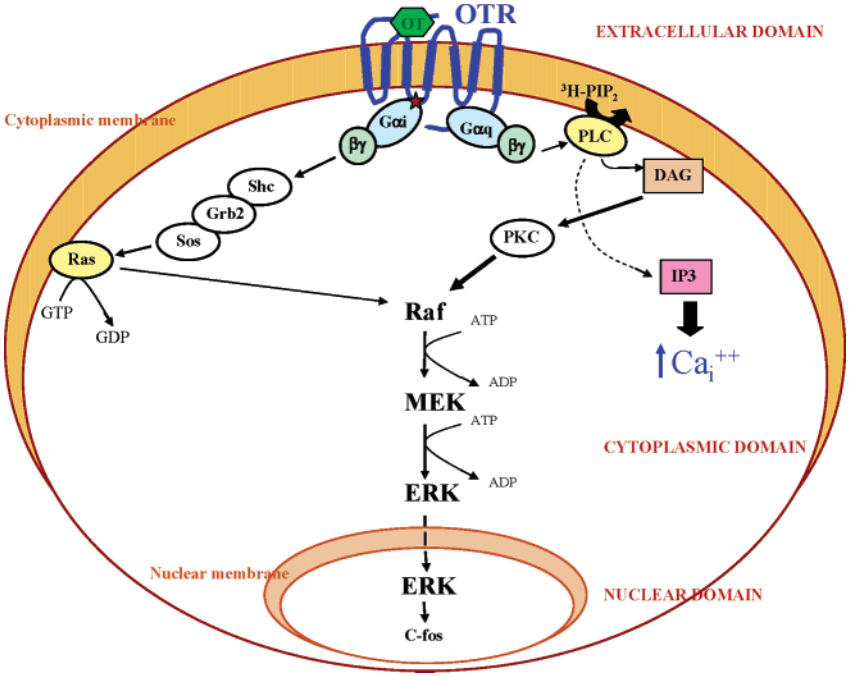

FIGURE 5: Signaling network. A schematic overview of a signaling network downstream of the OTR, emphasizing the pivotal role of the $G_{\alpha i}$−Ras−Raf−MAPK and $G_{\alpha q}$−PLC−IP3/Ca^{2+} signaling cascade, and the potential point of cross talk linking PLC−PKC−Raf to the MAPK cascade is shown. The red star denotes the D136N(3.49)N mutation.

0.7 nM) (Figure 4B). Thus, it would appear that D136(3.49)N lacks a high-affinity binding site observed in the WT receptor.

To further investigate whether the high-affinity binding site of the OTR was due to an interaction with $G\alpha_{i/o}$, we performed binding experiments following overnight incubation of COS-7 cells with PTX (200 ng/mL), which specifically ADP-ribosylates the $G\alpha_{i/o}$ subunit at the C-tail and therefore disrupts $G\alpha_{i/o}$−receptor coupling (*58*). High-affinity binding at the WT OTR was PTX sensitive and displayed one-site binding curves (Figure 4C) and a K_i value of 1.8 ± 0.2 nM, similar to that obtained in the presence of GTPγS. In contrast, at the D136(3.49)N mutant receptor, the monophasic binding and K_i (1.30 ± 0.2 nM) of OT remained unchanged (Figure 4D), suggesting that the D136(3.49)N mutation augments signaling through $G\alpha_q$ but disables the coupling of the OTR to $G\alpha_i$.

Because of the reports of the dual coupling of the OTR to $G\alpha_i$ and $G\alpha_q$ (*33*), we used an alternative approach to analyze the effect of the D136(3.49)N mutation on signaling properties by investigating the effect on the activation of Ras and PKC, activated by $G\alpha_i$ and $G\alpha_q$ pathways, respectively. Once activated, these kinases can then phosphorylate ERK1/2 in the nucleus of the cell (Figure 5). To investigate the $G\alpha_i$ component of this pathway, we studied the effect of PTX on p44/42 MAP kinase phosphorylation using a specific phospho ERK1/2 antibody [Phospho-p44/p42 MAP Kinase (Thr202/Tyr204) Antibody, Cell Signalling]. However, following the transfection of COS-7 cells with cDNAs encoding the WT or the D136(3.49)N OTR, no OT-mediated (200 nM) ERK1/2 phosphorylation could be detected due to a high basal level of phosphorylation (data not shown). Hence, we were unable to observe if PTX could affect ERK1/2 phosphorylation in these cell lines and decided to use HEK/EBNA cells transfected with either the WT or the D136(3.49) OTR. In comparison to mock transfected cells, transient transfection of the WT OTR resulted in an increase the basal level of ERK1/2 phosphorylation. The addition of OT (200 nM) rapidly increased the level of ERK1/2 phosphorylation further (Figure 6A). The maximal stimulation was achieved at around 5 min (data not shown). A 17 h pretreatment with PTX (300 ng/mL) reduced this level of OT-stimulated ERK1/2 phosphorylation, indicating that the majority of phosphorylation is PTX sensitive and mediated by $G\alpha_i$. Stimulation of the WT and or D136(3.49)N mutant cDNA with increasing concentrations of OT resulted in a dose-dependent increase in the level of stimulation of ERK1/2 phosphorylation. In contrast to the WT receptor, where PTX completely inhibited any OT-stimulated ERK1/2 phosphorylation in a statistically relevant manner ($p < 0.015$), the D136(3.49)N mutant-mediated stimulation was only slightly altered (Figure 6B). Thus, the D136(3.49)N mutant is dramatically impaired in its capability to stimulate cellular events mediated through activation of $G\alpha_i$ G proteins, suggesting that the D136(3.49)N receptor has a phenotype that expresses an enhanced ability to signal through $G\alpha_q$ G proteins while losing its ability to interact with $G\alpha_i$ G proteins.

Computational Modeling of the Free and OT-Bound Forms of the WT and Mutated OTR. In this study, in vacuo molecular simulations of the free and OT-bound forms of OTR were carried out to gain insight into the molecular mechanism of the structural information transfer from the hormone binding site (in the extracellular half of OTR) to the cytosolic domains. Moreover, molecular simulations of the free and OT-bound forms of the D136(3.49)N constitutively active mutant were instrumental in inferring hypotheses about the structural commonalities and differences between agonist- and mutation-induced active states as well as about the molecular determinants of the $G\alpha_q$ selectivity shown by the OT-stimulated D136(3.49)N mutant, as compared to the $G\alpha_i$ and $G\alpha_q$ promiscuity of the OT-stimulated WT. Com-

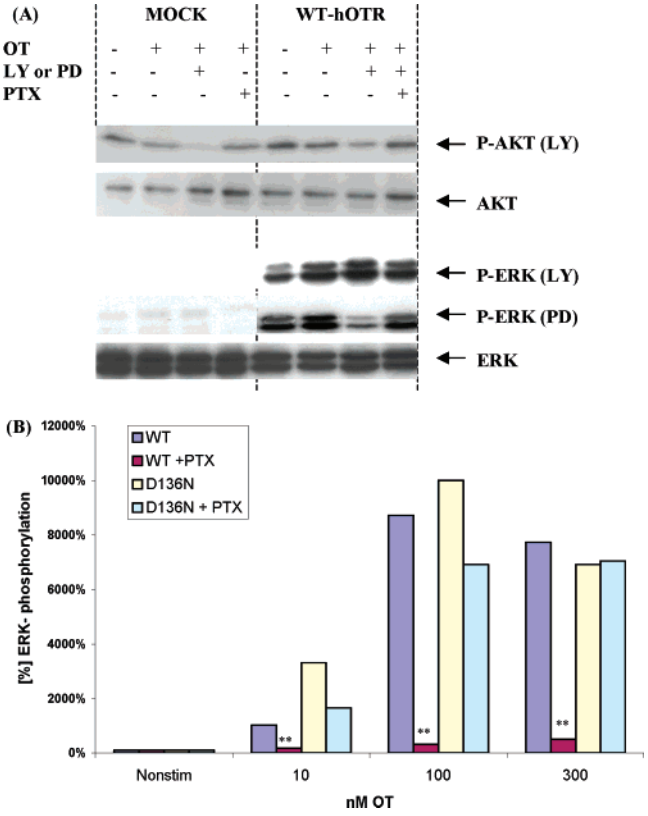

FIGURE 6: (A) Stimulation of ERK1/2 and AKT signaling by OT ligand using HEK/EBNA cells transiently transfected with hOTR-(WT). Cells were stimulated for 5 min with 200 nM OT in the presence or absence of pertussis toxin (PTX, 300 ng/mL, preincubation for 17 h prior to stimulation) and MEK inhibitor (PD98059, 10 μM, 20 min preincubation). Phosphorylation of AKT and ERK1/2 is shown by phospho specific antibody (P-AKT Ser473 and ERK Tyr202, Thr204, respectively). Expression was controlled by a non-phospho specific antibody (AKT, ERK). (B) Assessment of ERK1/2 phosphorylation via the dose−response relationship of OT in HEK/EBNA cells stably expressing the WT or the D136-(3.49)N mutant in the presence or absence of PTX. Cells were stimulated for 5 min with an increased concentration of OT in the presence or absence of pertussis toxin (PTX, 300 ng/mL, preincubation for 17 h prior to stimulation). The bar graph of ERK1/2 phosphorylation, using nonstimulated nontransfected cells as 100%, is shown. Expression was controlled by non-phospho specific ERK antibody. This graph represents a typical experiment, repeated four times (two asterisks indicates $p < 0.015$ for inhibition of ERK1/2 phosphorylation due to PTX at the WT OTR).

putations were carried out on the initial receptor model achieved by comparative modeling, by using the rhodopsin structure as a template (*41*).

Previous theoretical investigations on several GPCRs suggested that neighbors of the arginine of the E/DRY sequence are likely targets of the structural modifications induced by agonist or by activating mutations (*17*−*20*, *54*, *56*, *59*−*62*). Therefore, the interaction pattern of this fully conserved arginine is the main focus of the computational modeling herein presented, which essentially consists of comparative analyses of a large number of short (100 ps) and longer (1 ns) in vacuo MD trajectories, probing different input structures as well as different intrahelical distance restraints. Unrestrained MD simulations using an implicit membrane−water model (*51*) (i.e., IMM1 simulations) were additionally carried out to corroborate the results of computations. The mechanistic hypothesis inferred from this study is based upon the outcome of all the short and long MD runs that have been carried out. However, herein, only one rather representative long trajectory for each of the different forms of OTR will be discussed in more detail. For each receptor form, particular focus will be devoted to the few structural features, which make the difference between nonactive and active forms, overemphasizing the commonalities rather than the differences between in vacuo and IMM1 simulations.

Since 1 ns IMM1 trajectories have been produced also for the WT OTR carrying D136(3.49) protonated, in the following text, the terms WT OTR and D136(3.49)PROT will stand for OTR carrying the E/DRY aspartate in its unprotonated and protonated forms, respectively.

The selected in vacuo 1 ns trajectory of the unbound form of WT OTR is characterized by a persistent intrahelix charge-reinforced H-bond between R137(3.50), of the E/DRY motif, and the adjacent aspartate, D136(3.49). In the latest steps of simulation, the conserved arginine is additionally involved in a H-bonding interaction with T273(6.33). Such interhelical interaction substitutes, at least in part, for the interhelical salt bridge found in the rhodopsin structure between the homologous arginine and a glutamate at position 6.30 (Figure 7) (*41*). The same pattern of intramolecular interactions characterizes the IMM1 trajectory (Figure 8). Other features shared in common by the empty OTR structures derived by in vacuo and IMM1 simulations are H-bonding interactions involving highly conserved polar amino acids in the TM portion of helices 2 and 7, including interactions of D85-(2.50) with N325(7.49) and interactions of N321(7.45) with both W288(6.48) and N325(7.49) (Figures 7 and 8). However, we do not exclude the possibility that a water molecule might mediate the H-bonding interaction between D85(2.50) and N325(7.49) as suggested by the advances in the determination of rhodopsin structure (*63*).

The highly conserved tryptophan W288(6.48) also forms intrahelix van der Waals interactions with both F284(6.44) and F291(6.51) (Figures 7 and 8). The distances between the centers of the interacting aromatic rings in the average minimized structure obtained by in vacuo and IMM1 simulations are listed in Tables 3 and 4, respectively. In all the selected average minimized structures of the empty WT OTR, W288(6.48) is oriented so that its phenyl ring points toward F291(6.51) whereas the pyrrole ring points toward F284(6.44) (Figures 7 and 8). This interaction pattern of W288(6.48) is associated with a bend at P290(6.50), the fully conserved amino acid in helix 6 (*16*) (Figures 7 and 8). These interaction patterns are almost persistent during the whole MD simulation time. Another structural feature of the empty WT OTR is the interaction between Y329(7.51) of the NPxxY motif and F337 in helix 8 (Figures 7 and 8). The interaction between these two aromatic amino acids characterizes also the dark state of rhodopsin (*41*).

Both in vacuo and IMM1 trajectories of the D136(3.49)N constitutively active OTR mutant are characterized by the breakage of the salt bridge interaction found in the WT OTR between R137(3.50) and the adjacent D136(3.49) (Figures 7 and 8). The breakage of this intrahelix salt bridge is almost concurrent with the breakage of the interaction found in the empty WT between Y329(7.51), of the NPxxY motif, and F337 in helix 8 (Figures 7 and 8).

In the first 500 ps of MD simulations, the interaction pattern of D85(2.50), N321(7.45), and N325(7.49) is almost maintained as compared to that of the WT OTR (Figures 7

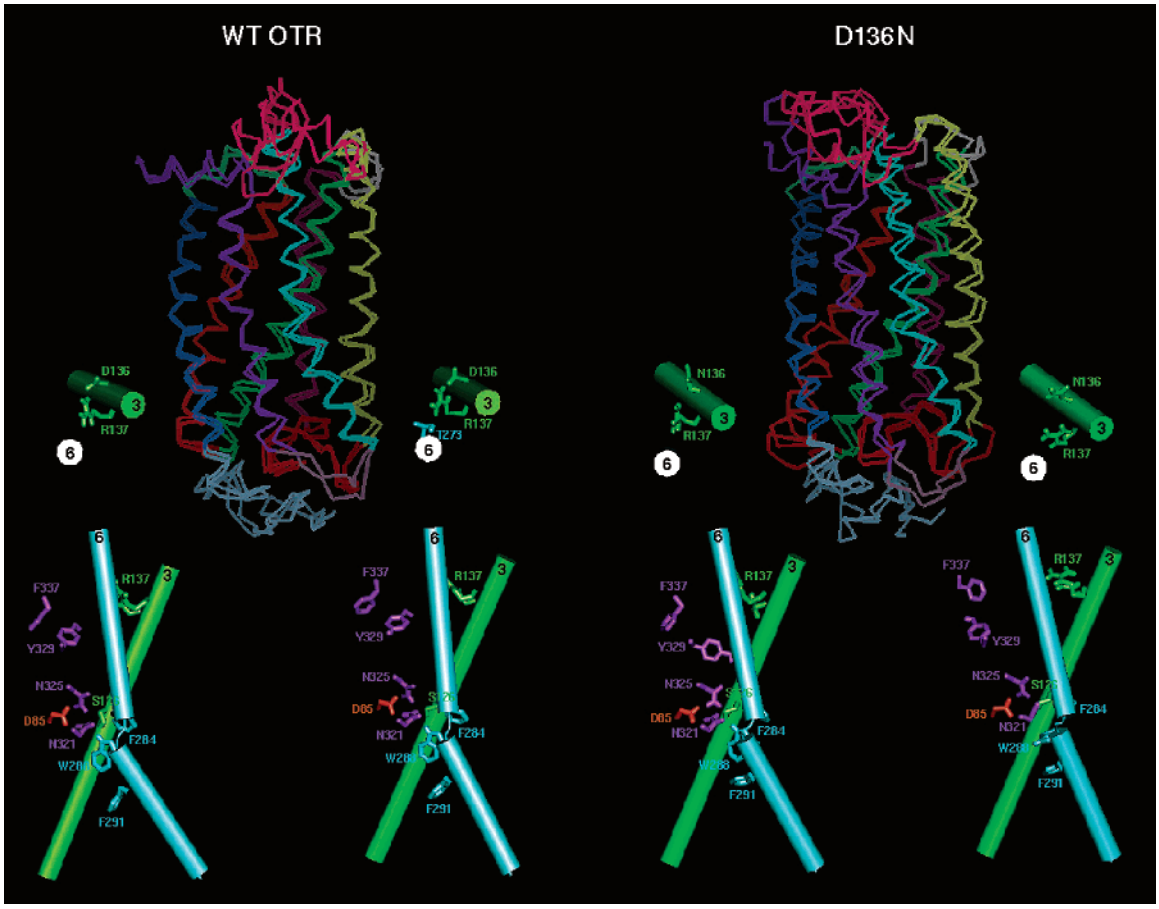

FIGURE 7: Average minimized structures of the empty forms of the WT OTR (left panel) and of the D136(3.49)N constitutively active mutant (right panel) achieved by in vacuo simulations. (Top) At the center of each panel, the superimposition of the structures averaged over the first and last 500 ps of the 1 ns MD trajectory and minimized is shown. Helices 1−7 are colored blue, orange, green, pink, yellow, cyan, and violet, respectively, whereas IL1−IL3 and EL1−EL3 are colored light green, white, cyclamen, red, purple, and gray, respectively. Helix 8 is colored violet like helix 7. The receptors are seen in a direction parallel to the membrane surface, the intracellular side being on top. On the left and right sides of the superimposed receptors, the cytosolic ends of helices 3 and 6 are shown which have been extracted from the structures averaged over the first and last 500 ps of the 1 ns MD trajectory, respectively. The two helices are seen from the intracellular side in a direction perpendicular to the putative membrane plane. Details of the interaction of the E/DRY arginine are also shown. (Bottom) Side view, in a direction parallel to the membrane surface, of helices 3 and 6 extracted from the structures averaged over the first (left side) and last (right side) 500 ps of the 1 ns MD trajectory. Details of the interactions of the E/DRY arginine, of selected polar conserved amino acids, and of the aromatic cluster in helix 6 are shown.

and 8). In IMM1 simulations, Y329(7.53) substitutes for D85(2.50) as the H-bonding partner of N325(7.49) (Figure 8). The reciprocal orientation of the members of the aromatic cluster in helix 6 does not diverge substantially from that found in WT OTR (Figures 7 and 8). In the in vacuo simulations, a perturbation occurs in the second half of the simulation, when W288(6.48) loses its H-bonding interaction with N321(7.45) and makes intrahelix $\pi-\pi$ staking interaction with F291(6.51) (Figure 7). Indeed, in the structure averaged over the last 500 ps, the distance between the centers of the pyrrole ring of W288(6.48) and the phenyl ring of F291(6.51) is 4.6 Å (Table 3). All the average minimized structures of the D136(3.49)N constitutively active mutant, especially those derived from IMM1 simulations, are characterized by a significant reduction in the bend at P290(6.50) (Figures 7 and 8), suggesting that the mutation at the cytosolic extension of helix 3 is able to transfer a structural modification in the extracellular half of helix 6, where the bend is located.

There is a significant overlapping in the average minimized structures of the D136(3.49)N mutant and those of D136(3.49)PROT concerning the interaction patterns of the conserved amino acids highlighted above (Figures 8 and 9).

Overall, the D136(3.49)N active mutant shows greater flexibility than the WT OTR (Figures 7 and 8). In fact, the rmsds between the main chain atoms of the structures averaged over the first and last 500 ps of in vacuo MD trajectory is 1.97 Å (i.e., 1.72 Å for IMM1 simulations) for the WT forms, whereas it is 3.28 Å (i.e., 2.57 Å for IMM1 simulations) for the D136(3.49)N active mutant. The same considerations are true for D136(3.49)PROT, which is more flexible in the cytosolic domains than the WT OTR; i.e., the rmsd between the main chain atoms of the structures averaged over the first and last 500 ps of the IMM1 trajectory is 2.29 Å.

In all of the >800 equilibrated MD trajectories of the OT−OTR complexes, the gross orientation of the hormone is such that the cyclic part of the ligand docks into a site constituted by EL2 as well as by the extracellular ends of helices 3, 6, and 7 (Figures 10−12). The linear part of the peptide docks into a site formed by the extracellular ends of helices 1 and 2 and by a few amino acids from the N-terminus, EL1, and EL2 (Figures 10−12).

The amino acids, which participate in OT binding, are quite overlapping in in vacuo and IMM1 simulations.

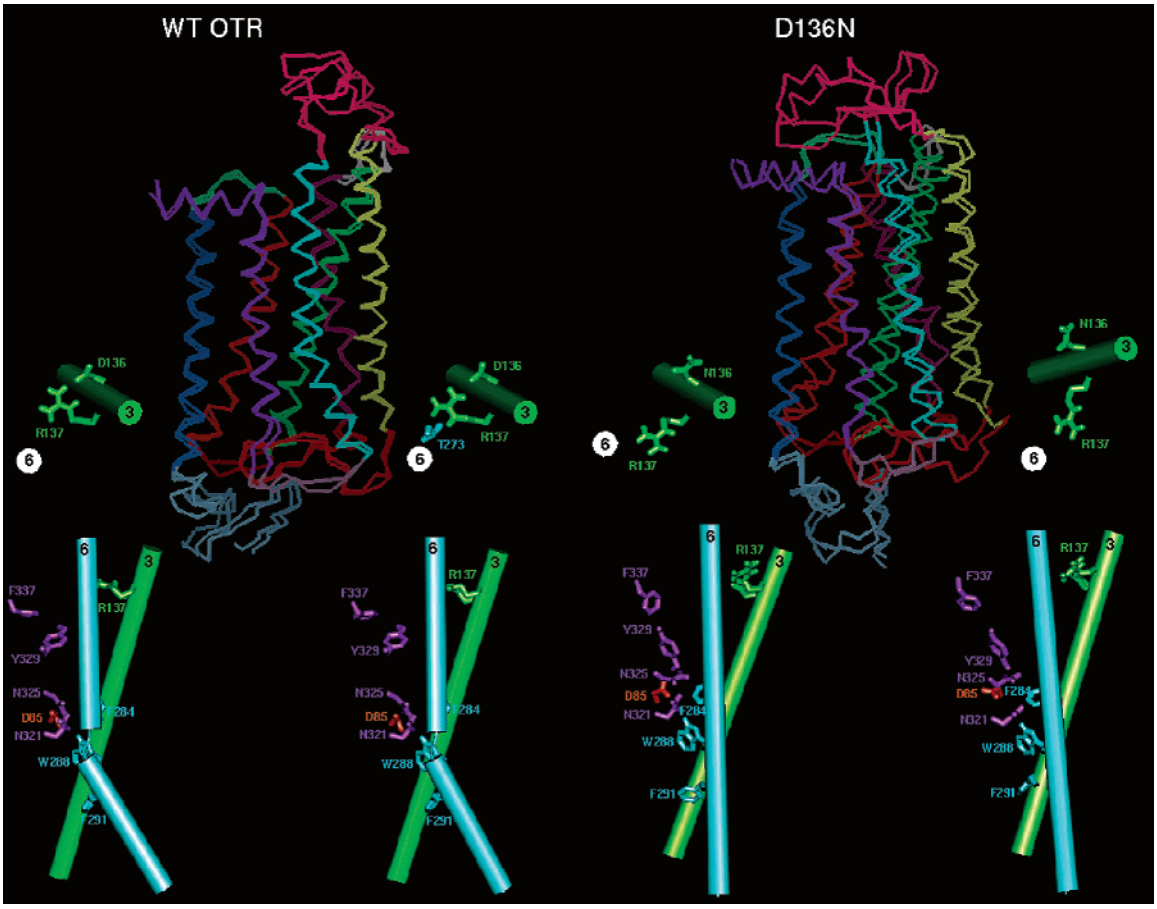

FIGURE 8: Average minimized structures of the empty forms of the WT OTR (left panel) and of the D136(3.49)N constitutively active mutant (right panel) achieved by IMM1 simulations. The description of this figure is like that of Figure 7.

Table 3: Distances between the Aromatic Centers of Tyr2, F291, W288, and F284

structure[a]	Tyr2−F291[b]	F291−W288[c]	W288−F284[d]
WT OTR_{f500}		6.5	4.5*
WT OTR_{l500}		5.9	4.6*
$D136N_{f500}$		4.5	4.4*
$D136N_{l500}$		4.6*	5.6*
OT−WT OTR_{f500}	5.0	5.9*	4.7
OT−WT OTR_{l500}	5.0**	6.6*	5.4
OT−$D136N_{f500}$	5.0	5.0	5.2*
OT−$D136N_{l500}$	5.1	7.3	4.8

[a] Structures of the wild-type OTR and the D136(3.49) active mutant in their free (WT OTR and D136N) and OT-bound (OT−WT OTR and OT−D136N) forms averaged over the first and last 500 ps of the in vacuo 1 ns trajectory (labeled f500 and l500, respectively). [b] Distances (angstroms) between the centers of the phenyl rings of Tyr2 of the hormone and F291(6.51) of the OTR. The double asterisk means that F292(6.52) substitutes for F291(6.51). [c] Distances (angstroms) between the centers of the phenyl rings of F291(6.51) and W288(6.48). The asterisk means that the center of the pyrrole ring of W288(6.48) is considered in the measurement. [d] Distances (angstroms) between the centers of the phenyl rings of W288(6.48) and F284(6.44). The asterisk means that the center of the pyrrole ring of W288(6.48) is considered in the measurement.

Table 4: Distances between the Aromatic Centers of Tyr2, F291, W288, and F284

structure[a]	Tyr2−F291[b]	F291−W288[c]	W288−F284[d]
WT OTR_{f500}		6.1	5.7*
WT OTR_{l500}		5.9	5.8*
$D136PROT_{f500}$		6.4	5.0*
$D136PROT_{l500}$		5.4	5.3*
$D136N_{f500}$		7.6	5.7*
$D136N_{l500}$		5.9*	5.7*
OT−WT OTR_{f500}	4.9	7.5*	4.8
OT−WT OTR_{l500}	5.6	5.9*	4.2*
OT−$D136PROT_{f500}$	6.7	7.4*	4.1
OT−$D136PROT_{l500}$	6.3	5.4	5.0*
OT−$D136N_{f500}$	5.4	6.6	5.6
OT−$D136N_{l500}$	5.3	6.8	5.0

[a] Structures of the wild-type OTR carrying D136(3.49) unprotonated (WT OTR) and protonated (D136PROT) as well as the D136(3.49)N active mutant in their free and OT-bound (OT−WT OTR, OT−D136PROT, and OT−D136N) forms averaged over the first and last 500 ps of the IMM1 1 ns trajectory (labeled f500 and l500, respectively). [b] Distances (angstroms) between the centers of the phenyl rings of Tyr2 of the hormone and F291(6.51) of the OTR. The double asterisk means that F292(6.52) substitutes for F291(6.51). [c] Distances (angstroms) between the centers of the phenyl rings of F291(6.51) and W288(6.48). The asterisk means that the center of the pyrrole ring of W288(6.48) is considered in the measurement. [d] Distances (angstroms) between the centers of the phenyl rings of W288(6.48) and F284(6.44). The asterisk means that the center of the pyrrole ring of W288(6.48) is considered in the measurement.

However, the details of interactions are different and can vary even within the same trajectory. Almost constant elements in the trajectories of the OT−OTR complexes are the interactions between Tyr2 of OT and both F291(6.51) and Q295(6.55) of OTR (Figure 12). In some of the in vacuo MD trajectories, the C-terminus of OT is involved in interaction with R34 (at the boundary between the N-terminal tail and helix 1), an amino acid that has been demonstrated to be required for high-affinity agonist binding (*47*, *48*). Indeed, this interaction is persistent in the majority of

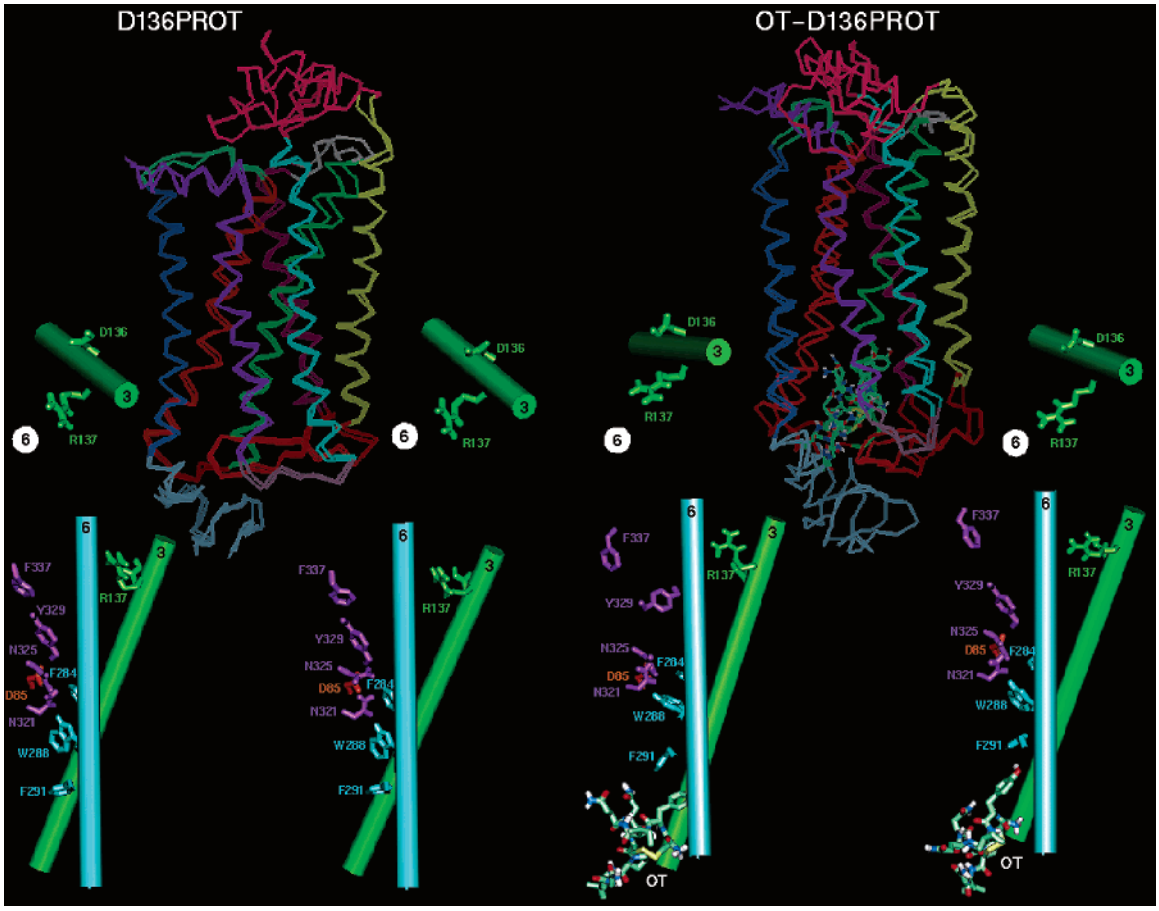

FIGURE 9: Average minimized structures of the empty (left panel) and OT-bound (right panel) forms of D136(3.49)PROT achieved by IMM1 simulations. The description of this figure is like that of Figure 7.

the IMM1 trajectories, probably because R34 has more degrees of freedom, due to the lack of intrahelix distance restraints.

The OT orientations proposed in this study are similar to ones previously reported (*19*). However, there are detailed intermolecular interactions that are different because of inconsistencies in the arrangements of the extracellular domains of the OTR, which in this study are based on the crystal structure of rhodopsin (*41*). Despite the differences between the old and new OTR models, they both suggest that R137(3.50) is the target of the structural modifications induced by OT.

Molecular simulations carried out on the OT-bound forms of the WT OTR suggest that the optimization of intermolecular interactions between Tyr2 of the ligand and F291(6.51), amino acids, which have been, respectively, shown to be important for OT and GPCR function (*49*, *50*), is concurrent with the breakage of the intrahelix charge-reinforced H-bond, which involves the arginine of the E/DRY motif in the empty WT OTR (Figures 7−11). The transfer of the structural modifications from the extracellular side to the intracellular domains is mediated by the cluster of aromatic amino acids in helix 6, formed by F291(6.51), W288(6.48), and F284(6.44). In this respect, the information transfer is suggested to be triggered by orthogonal $\sigma-\pi$ interaction between Tyr2 of the ligand and F291(6.51) (Figures 10−12). This interaction, which is suggested to be favored by the concomitant establishment of an intermolecular H-bond between Tyr2 and Q295(6.55), induces a change in the conformation and interaction pattern of W288(6.48), as compared to that of the empty OTR (Figures 7, 8, 10, and 11). Indeed, W288(6.48) detaches from F291(6.51), reinforcing its interaction with F284(6.44) (Tables 3 and 4). This is particularly true for IMM1 simulations, which showed a recurrent increase in distance between the centers of the phenyl rings of F291(6.51) and W288(6.48), correlated with the presence of the intermolecular interaction between Tyr2 of the hormone and F291(6.51) of the receptor (Tables 3 and 4 and Figures 10 and 11). This effect is due, at least in part, to a rotation of the plane of the indole ring of W288(6.48) from an almost perpendicular to an almost parallel orientation with respect to the putative membrane surface (Figures 7−11). The rearrangement of W288(6.48) is associated with a reduction of the bend at P290(6.50), found in the empty OTR (Figures 7, 8, 10, and 11).

In a manner different from that of the OT-bound forms of WT OTR, for the OT-bound forms of the D136(3.49)N mutant and of D136(3.49)PROT, the establishment of the Tyr2-F291(6.51) intermolecular interaction appears to be less relevant for the perturbation of the interaction pattern of the E/DRY arginine, which instead is triggered by the irreversible or reversible charge neutralization of D136(3.49) (Figures 7−11).

As for the H-bonds that involve the polar conserved amino acids in helices 2 and 7, the difference between free and OT-bound forms, for which consensus exists between in vacuo and IMM1 simulation, is the H-bond between W288-

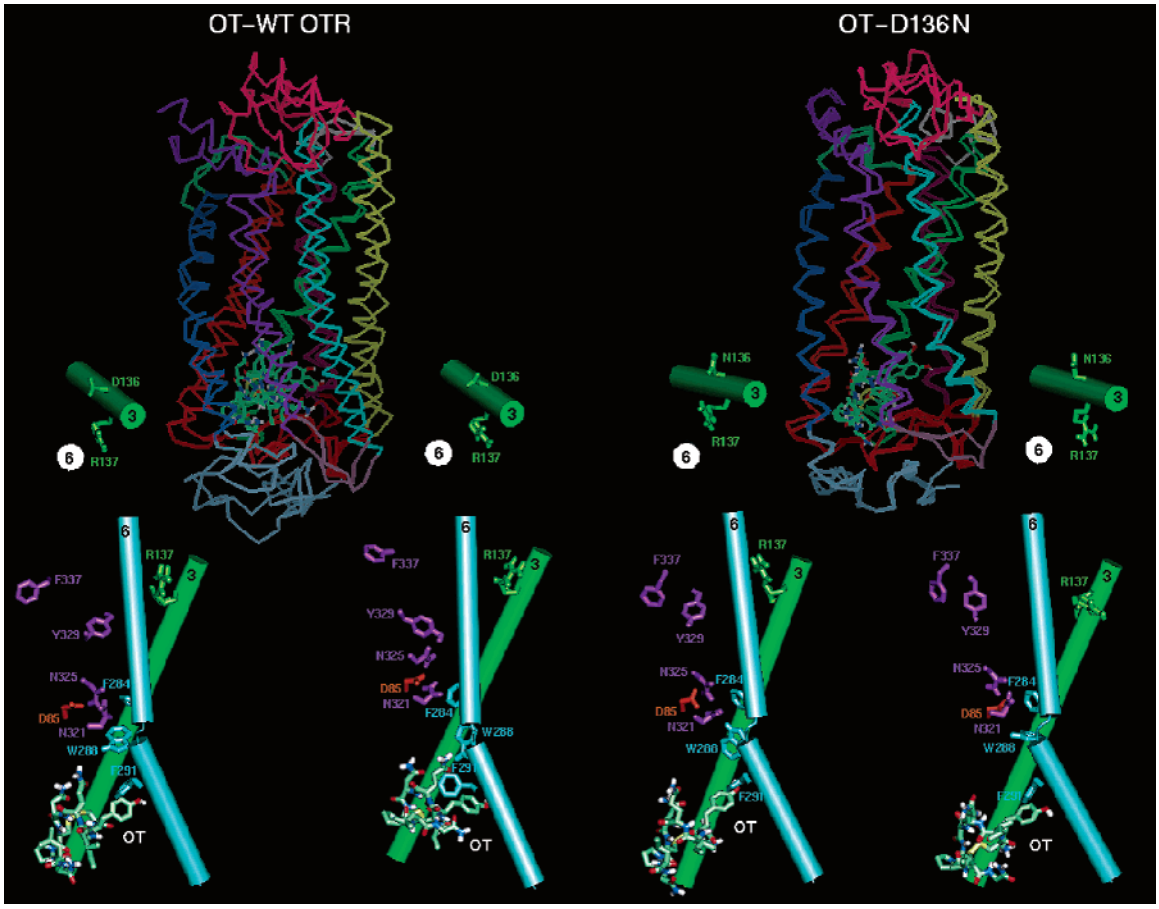

FIGURE 10: Average minimized structures of the OT-bound forms of WT OTR (left panel) and of the D136(3.49)N constitutively active mutant (right panel) achieved by in vacuo simulations. The description of this figure is like that of Figure 7.

(6.48) and N321(7.45) absent in the hormone−receptor complexes (Figures 7, 8, 10, and 11).

In the OT-bound forms of WT OTR and D136(3.49)-PROT, the breakage of the D136(3.49)−R137(3.50) charge-reinforced H-bond is always concurrent with the weakening of the interaction found in the empty WT OTR between Y329(7.51), of the NPxxY motif, and F337, in helix 8 (Figures 7−11).

Overall, OT binding significantly increases the structural flexibility of the WT OTR. In fact, the rmsd between the main chain atoms of the structures averaged over the first and last 500 ps of the MD trajectory is 1.97 Å (i.e., 1.72 Å for IMM1 simulations) for the empty WT OTR, whereas it is 3.32 Å (i.e., 2.98 Å for IMM1 simulations) for the OT-bound form. The mobility of the OT−D136(3.49)PROT complex is comparable to that of the OT−WT OTR complex, i.e., a rmsd of 2.71 Å compared to a rmsd of 2.98 Å. In contrast, the structural flexibility of the OT-bound form of the constitutively active mutant is lower than that of the OT-bound form of the WT OTR. The rmsd between the main chain atoms of the structures averaged over the first and last 500 ps of the MD trajectory of the OT−D136(3.49)N complexes is 2.44 Å (i.e., 1.39 Å for IMM1 simulations).

DISCUSSION

Mutagenesis studies have provided valuable insights into receptor domains critical for G protein coupling and activation, but as yet, conserved sequences driving these processes have not been identified (*1*, *3*, *8*, *64*). Constitutively active receptor mutants have been widely used as tools to investigate GPCR function as they were thought to mimic, at least in part, the agonist-bound (i.e., active) state of a GPCR, adopting a configuration capable of interacting with one or more G proteins (*66*).

Currently, the most widely accepted thermodynamic model of agonist- and mutation-induced GPCR activation is the extended ternary complex model (*67*−*70*), which predicts that receptors can exist in equilibrium between an inactive (R) and an active (R*) conformation that differ in their ability to activate G proteins. According to these models, agonist binding or constitutively active mutations shift the equilibrium toward R*. However, the complex behavior of GPCRs has now led to predictions that receptors can exist in multiple states each of which can couple to distinct G proteins (*17*, *71*−*75*). Consistent with this idea, mutation-induced and agonist-induced active states may be different as suggested by the discovery that some constitutively active mutants did not exhibit increased levels of phosphorylation as observed for the agonist-stimulated WT receptors (*17*, *18*, *76*).

Surprisingly, very little alteration in amino acid sequence is needed for a change in G protein selectivity. Indeed, point mutations of the LH (*77*), histamine H2 (*24*), and α_2-adrenergic (*10*) receptors were shown to uncouple the interaction with one G protein subtype while retaining the ability to couple to another subtype. Structural elements important for $G\alpha_q$ coupling in the OTR were identified by mutagenesis experiments, in which substitution of sequences from the cytosolic domains of the $G\alpha_s$-coupled vasopressin

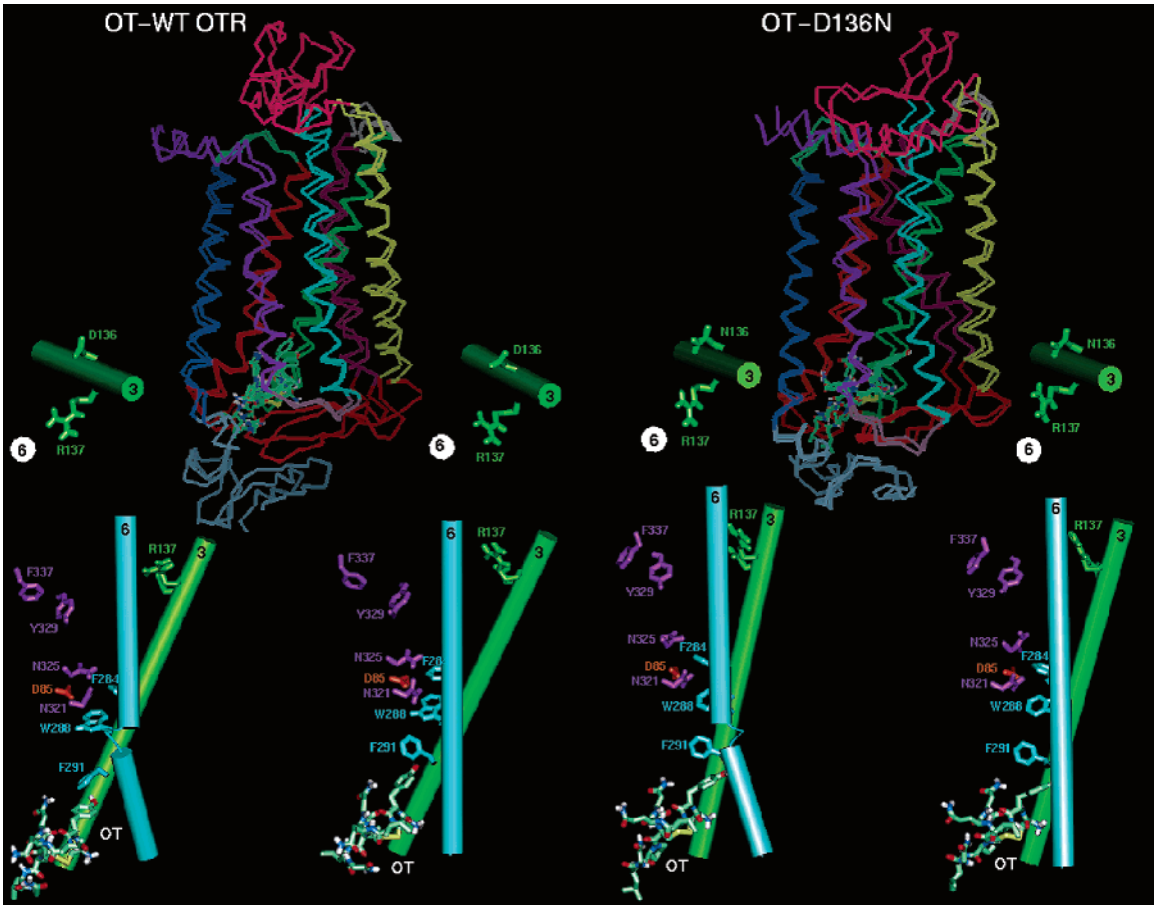

FIGURE 11: Average minimized structures of the OT-bound forms of the WT OTR (left panel) and of the D136(3.49)N constitutively active mutant (right panel) as achieved by IMM1 simulations. The description of this figure is like that of Figure 7.

V2 receptor into homologous positions in the OTR markedly reduced ligand affinity and abolished $G\alpha_q$ coupling (*38*).

With the aim of finding novel constitutively active mutants useful in investigating deeply the G protein coupling features of the human OTR, we mutated amino acid residues found to be susceptible to activating mutations in other GPCRs (Table 1) (*19*, *22*−*26*, *52*−*58*). Pharmacological characterization of these OTR mutants revealed an expression level significantly lower than that of the WT receptor, likely to be due to either structural instability or incorrect protein folding (*78*−*80*). Indeed, expression of seven of the mutants was too weak to allow further characterization, and of the remaining five that did express, only the D136(3.49)N mutant could exhibit an increased level of OT-stimulated IP3 accumulation. Surprisingly, we were not able to detect expression of the R137(3.50)A mutant, which was previously reported to be constitutively active (*19*). The homologous mutation in the vasopressin V2 receptor and in other GPCRs resulted in profoundly impaired expression as well (*17*, *81*−*85*).

As shown for other GPCRs (*17*, *18*, *20*, *22*−*26*), a mutation of the aspartate of the DRY motif resulted in the D136(3.49)N OTR exhibiting constitutive activity through the $G\alpha_q$ pathway. This mutated receptor, despite being expressed at approximately half the level of the WT receptor, demonstrated a significantly elevated basal level and an increased potency for OT to stimulate IP3 accumulation, compared with the WT receptor. At a comparable receptor density, the basal level of IP3 accumulation of the D136(3.49)N mutant could be even higher, as previously shown for the constitutively active histamine H2 receptor (*24*). The partial agonist AVP became a full agonist at the D136(3.49)N receptor, and as with OT, the potency to stimulate IP3 accumulation was increased. This is in contrast to the previously reported constitutively active R137(3.50)A OTR mutant (*19*) which possessed an increased basal IP3 activity but no increase in agonist potency. Hence, a mutation of the aspartate residue of the DRY motif into asparagine produced what we believe to be the first highly constitutively active OTR mutant. Consistent with reports of other constitutively active receptors (*19*, *68*, *71*), we did not observe any differences in the binding affinity of OT between the WT and D136(3.49)N receptor, suggesting that the extent to which agonist binding is affected may be highly variable and ligand specific.

Very little is known about the role of MAPK in OT action. Previous work has shown that OT treatment caused the rapid phosphorylation of ERK2, which was partially inhibited by PTX, consistent with OTR−$G\alpha_i$ coupling. The PTX insensitive portion of ERK2 phosphorylation was linked to $G\alpha_q$, as inhibitors of both phospholipase C and protein kinase C blocked OT-induced ERK2 phosphorylation (*33*). To investigate the effect of the D136(3.49)N mutation on the alternative $G\alpha_i$ signaling pathway, we measured phosphorylation of ERK1/2 in HEK/EBNA cells. For the WT OTR, phosphorylation of p44-p42 MAP kinase occurred through both PTX sensitive and PTX insensitive pathways. In contrast, for the D136(3.49)N mutant, no effect of PTX was

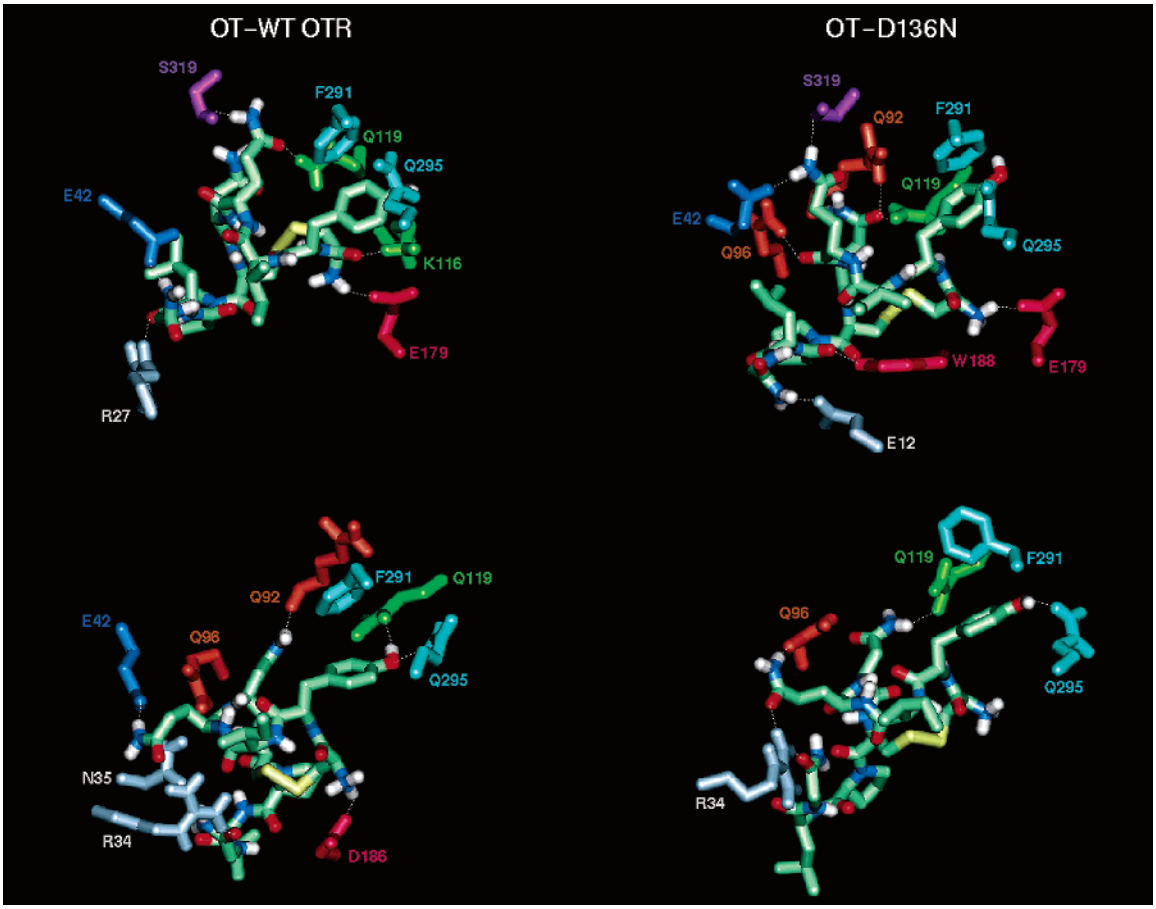

FIGURE 12: Structures of the OT-bound forms of WT OTR (left panel) and D136(3.49)N mutant (right panel) averaged over the first 500 ps of in vacuo (top) and IMM1 (bottom) 1 ns simulations. Selected receptor amino acids involved in H-bonding interactions with OT are shown. Manually drawn dashed lines represent the hydrogen bonds. The interaction between Tyr2 of the hormone and F291(6.51) of the receptor is also shown.

observed, suggesting that this receptor was no longer able to couple to $G\alpha_i$.

The constitutively active lipid receptor SIP5 has the ability to stimulate various effector pathways, but each pathway to a different extent (*86*). However, mutations have been reported that cause receptor-mediated constitutive coupling largely restricted to the activation of one single signaling pathway. The other signaling properties observed in the promiscuous WT receptor were either unaffected or impaired (*7*, *71*, *86*−*89*). Thus, such mutations are likely to stabilize selected active states of OTR, indicating that activation of multiple signaling is likely to result from independent coupling with distinct G proteins. Our D136(3.49)N receptor mutant appeared to exist in a high-affinity state with an attenuated ability to activate the $G\alpha_i$ protein but a constitutive activity toward the $G\alpha_q$ pathway. This suggests that while D136(3.49) is required for coupling to $G\alpha_i$ pathways, it is also required to keep receptor in a "constrained" state and prevent constitutive activation. The ability to couple solely to one G protein subtype, likely due to a change in the conformation of the cytosolic domains, would suggest that the D136(3.49)N mutated receptor has determinants that steer it away from other G protein subtypes that are not desired.

Computational modeling done before and after the availability of rhodopsin structure on the α_{1b}-AR (*14*, *17*, *18*, *20*, *54*, *56*), the LHR (*61*, *62*), the OTR (*19*), the 5-HT_{1A} serotonine receptor (*59*), and melanin-concentrating hormone receptors (*60*) converged into the hypothesis that the receptor portions close to the E/DRY and NPxxY motifs are particularly susceptible to undergoing structural modification in response to activating mutations and to agonist binding. The results of experiments and simulations carried out in this study further corroborate this hypothesis. In fact, both in vacuo and IMM1 simulations show that OT binding, D136(3.49) protonation, and the D136(3.49)N mutation can break the interactions found in the unbound WT OTR between R137(3.50) and both D136(3.49) and T273(6.33) (Figures 7−11). The interaction of R137(3.50) with T273-(6.33) substitutes, at least in part, for the interhelical salt bridge found in the rhodopsin structure between the homologous arginine and E247(6.30) (Figures 7−10). The latter was suggested to be important for stabilizing the inactive states of the α_{1b}-adrenergic (*54*, *56*), β_2-adrenergic (*55*), and 5-HT_{2A} serotonin (*90*, *91*) receptors. Indeed, replacing E6.30 in the α_{1b}-adrenergic receptor with lysine was demonstrated to induce a very high level of constitutive activity (*54*, *56*). Interestingly, in the OTR, the homologous residue is a lysine that was shown to be essential for $G\alpha_q$ coupling specificity (*38*). In agreement with a recent study on the μ-opioid receptor (*92*), our results suggest that, in the absence of a conserved glutamate/aspartate at position 6.30, other amino acids in the cytosolic extension of helix 6 may contribute to the creation of H-bonding interactions with the E/DRY arginine. This provides stronger support to the hypothesis that it is the Asp of the E/DRY motif that plays a more important role in stabilizing the inactive state of GPCRs

compared with the less conserved glutamic/aspartic amino acid in helix 6.

Other perturbations in the cytosolic domains that are shared by the empty D136(3.49)PROT, D136(3.49)N mutant, and OT-bound forms of nonmutated OTR include a destabilization of the interaction found in the empty receptor between Y329(7.51), of the NPxxY motif, and F337, in helix 8 (Figures 7−11). These results are consistent with recent experimental evidence on rhodopsin activation, indicating that the $NPxxY(x)_{5,6}F$ and D/ERY motifs provide, in concert, a dual control of the activating structural changes in the photoreceptor (*94*).

In agreement with recent computational modeling studies on the $5\text{-}HT_{1A}$ serotonin and the melanin-concentrating hormone receptors (*59, 60*), in the WT OTR, the agonist-induced transfer of the structural modification from the extracellular side to the cytosolic domains is suggested to be mediated by a cluster of aromatic amino acids in helix 6 [i.e., F284(6.44), W288(6.48), and F291(6.51)]. In this respect, the most productive intermolecular interactions include the orthogonal $\sigma-\pi$ interactions between Tyr2 of the ligand and F291(6.51) of the OTR, an interaction that is not always persistent over the entire simulation time and that is favored by Q295(6.55). The hypothesis inferred from computations is that such intermolecular interaction is instrumental in perturbing the aromatic cluster in helix 6, by making W288(6.48) lose its interhelical H-bond with N321(7.45) and weaken its intrahelix interaction with F291-(6.51), thus reinforcing its interaction with F284(6.44), the most intracellular and conserved member of the aromatic cluster in helix 6 (Figures 7−11 and Tables 3 and 4). The side chain movements of W288(6.48) are associated with a significant reduction in the bend at P290(6.50), as compared to that of the empty WT OTR (Figures 7−11).

In contrast, in the OT-bond forms carrying D136(3.49) protonated or mutated into asparagine, perturbations of the D136(3.49)−R137(3.59) interaction are suggested to be triggered by the neutralization of the E/DRY aspartate rather than by the structural change triggered by the agonist. This hypothesis comes, at least in part, from the observation that the optimization of peculiar hormone−receptor interactions, including that between Ty2 and F291(6.51), is not necessary for perturbation of the ground state arrangement of the E/DRY motif.

Despite the similarities between them, the OT-bound forms of the WT OTR and of the D136(3.49)N constitutively active mutant show clear structural differences. In general, the OT-bound form of the WT OTR is characterized by higher mobility than the OT-bound form of the D136(3.49)N constitutively active mutant (Figures 7−10). This suggests that the former explores a larger number of states than the latter. Most importantly, the accessibility of the OT-bound form of WT OTR to a higher number of states, as compared to the OT-bound form of D136(3.49)N, can be also due to the possibility that the aspartate at position 3.49 can exist in both the nonprotonated (anionic) and protonated (neutral) forms, whereas the asparagine can exist in only the neutral state. Indeed, MD simulations suggest that protonation of D136(3.49) makes the WT receptor explore a higher number of different active states as compared to the D136(3.49)N mutant. All together, these features correlate with the higher degree of G protein coupling promiscuity of the OT-bound form of WT OTR as compared to the OT-bound form of the active mutant. Molecular simulations cannot say more about the G protein selectivity/promiscuity issue also because the C-tail of OTR, which could play a role in G protein recognition, has not been modeled.

Theory now suggests that the selectivity of G protein coupling is maintained by a combination of an "activation domain" and a "selectivity domain", each of which promotes and restricts coupling of GPCR to multiple G protein subtypes, respectively. These two domains are predicted to define the conformation of the intracellular region of GPCRs, and as such, any slight change in conformation at these two functional domains could affect the fidelity of G protein coupling (*94*).

Multiple-state models could also explain the differences in the efficiency of an agonist in coupling to distinct signaling cascades as a result of possessing different affinities for distinct active states (*95*). This concept of "agonist-specific trafficking or receptor signaling" (*96, 97*) is poorly understood, but there is much evidence that receptor coupling to different signaling pathways is dependent upon expression levels of receptor, cognate G protein, and/or different signaling molecules in different cellular models (*98*).

The cubic ternary model (*99*) explains the action of these "biased agonists" as an ability to stabilize distinct active and inactive states of G proteins to stimulate and inhibit G protein pathways, respectively. The final agonist response will be governed by its preference for these states and the relative amount of G proteins available. Pharmacological diversity may thus be achieved by the development of signaling specific therapeutic compounds that induce a single receptor conformation able to interact with distinct G proteins.

In conclusion, our results extend further the hypothesis that the E/DRY motif, in addition to a crucial role as a molecular switch toward receptor activation, acts also as a key determinant in stabilizing a specific conformation for the selective interaction with different G proteins. No $G\alpha_i$ signaling could be monitored with the D136(3.49)N mutated receptor, while the activity via $G\alpha_q$ pathways was markedly enhanced, suggesting that D136(3.49) is required both to keep the receptor "constrained" to prevent constitutive activation and to couple to $G\alpha_i$ pathways. This may involve different oligomeric states of the receptor, consistent with an ever-growing body of evidence that shows that signal transduction pathways can be modulated by differential GPCR aggregation (*100, 101*).

ACKNOWLEDGMENT

We thank Drs. Susanna Cotecchia and André Chollet for helpful suggestions. We are also very grateful to T. Lazaridis, E. Paci, and M. Seeber for letting us probe the IMM1 energy function. Technical support from CICAIA (Centro Interdipartimentale di Calcolo Automatico ed Informatica Applicata), University of Modena and Reggio Emilia, is acknowledged (F.F.).

REFERENCES

1. Wess, J. (1997) G-protein-coupled receptors: Molecular mechanisms involved in receptor activation and selectivity of G-protein recognition, *FASEB J. 11*, 346−354.
2. Bockaert, L., and Pin, J. P. (1999) Molecular tinkering of G protein-coupled receptors: An evolutionary success, *EMBO J. 18*, 1723−1729.

3. Gether, U. (2000) Uncovering molecular mechanisms involved in activation of G protein-coupled receptors, *Endocr. Rev. 21*, 90−113.
4. Federman, A. D., Conklin, B. R., Schrader, K. A., Reed, R. R., and Bourne, H. R. (1992) Hormonal stimulation of adenylyl cyclase through Gi-protein $\beta\gamma$ subunits, *Nature 356*, 159−161.
5. Allgeier, A., Offermanns, S., Van Sande, J., Spicher, K., Schultz, G., and Dumont, J. E. (1994) The human thyrotropin receptor activates G-proteins Gs and Gq/11, *J. Biol. Chem. 269*, 13733−13735.
6. Herrlich, A., Kühn, B., Grosse, R., Schmid, A., Schultz, G., and Gudermann, T. (1996) Involvement of Gs and Gi proteins in dual coupling of the luteinizing hormone receptor to adenylyl cyclase and phospholipase C, *J. Biol. Chem. 271*, 16764−16772.
7. Abadji, V., Lucas-Lenard, J. M., Chin, C., and Kendall, D. A. (1999) Involvement of the carboxyl terminus of the third intracellular loop of the cannabinoid CB1 receptor in constitutive activation of Gs, *J. Neurochem. 72*, 2032−2038.
8. Möller, S., Vilo, J., and Croning, M. D. R. (2001) Prediction of the coupling specificity of G protein coupled receptors to their G proteins, *Bioinformatics 17* (Suppl. 1), S174−S181.
9. Iida-Klein, A., Guo, J., Xie, L. Y., Jüpper, H., Potts, J. T., Jr., Kronenberg, H. M., Bringhurst, F. R., Abou-Samra, A. B., and Segre, G. V. (1995) Truncation of the carboxyl-terminal region of the rat parathyroid hormone (PTH)/PTH-related peptide receptor enhances PTH stimulation of adenylyl cyclase but not phospholipase C, *J. Biol. Chem. 270*, 8458−8465.
10. Eason, M. G., and Liggett, S. B. (1996) Truncation of the carboxyl-terminal region of the rat parathyroid hormone (PTH)/PTH-related peptide receptor enhances PTH stimulation of adenylyl cyclase but not phospholipase C, *J. Biol. Chem. 271*, 12826−12832.
11. Verrall, S., Ishii, M., Chen, M., Wang, L., Tram, T., and Coughlin, S. R. (1997) Truncation of the carboxyl-terminal region of the rat parathyroid hormone (PTH)/PTH-related peptide receptor enhances PTH stimulation of adenylyl cyclase but not phospholipase C, *J. Biol. Chem. 272*, 6898−6902.
12. Näsman, J., Jansson, C. C., and Åkerman, K. E. O. (1997) The second intracellular loop of the α2-adrenergic receptors determines subtype-specific coupling to cAMP production, *J. Biol. Chem. 272*, 9703−9708.
13. Lichtarge, O., Bourne, H. R., and Cohen, F. E. (1996) Evolutionarily conserved G$\alpha\beta\gamma$ binding surfaces support a model of the G protein-receptor complex, *Proc. Natl. Acad. Sci. U.S.A. 93*, 7507−7511.
14. Fanelli, F., Menziani, M. C., Scheer, A., Cotecchia, S., and De Benedetti, P. G. (1999) Theoretical study of the electrostatically driven step of receptor-G protein recognition, *Proteins: Struct., Funct., Genet. 37*, 145−156.
15. Oliveira, L., Paiva, A. C., and Vriend, G. (1999) Theoretical study of the electrostatically driven step of receptor-G protein recognition, *Protein Eng. 12*, 1087−1095.
16. Mirzadegan, T., Benko, G., Filipek, S., and Palczewski, K. (2003) Sequence Analyses of G Protein-Coupled Receptors: Similarities to Rhodopsin, *Biochemistry 42*, 2759−2767.
17. Scheer, A., Fanelli, F., Costa, T., De Benedetti, P. G., and Cotecchia, S. (1996) Constitutively active mutants of the α1B-adrenergic receptor: Role of highly conserved polar amino acids in receptor activation, *EMBO J. 15*, 3566−3578.
18. Scheer, A., Fanelli, F., Costa, T., De Benedetti, P. G., and Cotecchia, S. (1997) The activation process of the α1B-adrenergic receptor: Potential role of protonation and hydrophobicity of a highly conserved aspartate, *Proc. Natl. Acad. Sci. U.S.A. 94*, 808−813.
19. Fanelli, F., Barbier, P., Zanchetta, D., De Benedetti, P. G., and Chini, B. (1999) Activation mechanism of human oxytocin receptor: A combined study of experimental and computer-simulated mutagenesis, *Mol. Pharmacol. 56*, 214−225.
20. Scheer, A., Costa, T., Fanelli, F., De Benedetti, P. G., Mhaouty-Kodja, S., Abuin, L., Nenniger-Tosato, M., and Cotecchia, S. (2000) Mutational analysis of the highly conserved arginine within the Glu/Asp-Arg motif of the α_{1b}-adrenergic receptor: Effects on receptor isomerization and activation, *Mol. Pharmacol. 57*, 219−231.
21. Wilbanks, A. M., Laporte, S. A., Bohn, L. M., Barak, L. S., and Caron, M. G. (2002) Apparent loss-of-function mutant GPCRs revealed as constitutively desensitized receptors, *Biochemistry 41*, 11981−11989.
22. Cohen, G. B., Yang, T., Robinson, P. R., and Oprian, D. D. (1993) Constitutive activation of opsin: Influence of charge at position 134 and size at position 296, *Biochemistry 32*, 6111−6115.
23. Rasmussen, S. G., Jensen, A. D., Liapakis, G., Ghanouni, P., Javitch, J. A., and Gether, U. (1999) Mutation of a highly conserved aspartic acid in the β_2 adrenergic receptor: Constitutive activation, structural instability, and conformational rearrangement of transmembrane segment, *Mol. Pharmacol. 56*, 175−184.
24. Alewijnse, A. E., Timmerman, H., Jacobs, E. H., Smit, M. J., Roovers, E., Cotecchia, S., and Leurs, R. (2000) The effect of mutations in the DRY motif on the constitutive activity and structural instability of the histamine H_2 receptor, *Mol. Pharmacol. 57*, 890−898.
25. Morin, D., Cotte, N., Balestre, M. N., Mouillac, B., Manning, M., Breton, C., and Barberis, C. (1998) The D136A mutation of the V_2 vasopressin receptor induces a constitutive activity which permits discrimination between antagonists with partial agonist and inverse agonist activities, *FEBS Lett. 441*, 470−475.
26. Lu, Z. L., Curtis, C. A., Jones, P. G., Pavia, J., and Hulme, E. C. (1997) The D136A mutation of the V_2 vasopressin receptor induces a constitutive activity which permits discrimination between antagonists with partial agonist and inverse agonist activities, *Mol. Pharmacol. 51*, 234−241.
27. Soloff, M. S., Alexandrova, M., and Fernstrom, M. J. (1979) Oxytocin receptors: Triggers for parturition and lactation? *Science 204*, 1313−1315.
28. Fuchs, A. R., Fuchs, F., Husselein, P., and Soloff, M. (1984) Oxytocin receptors in the human uterus during pregnancy and parturition, *Am. J. Obstet. Gynecol. 150*, 734−741.
29. Williams, P. D., Ball, R. G., Clineschmidt, B. V., Culberson, J. C., Erb, J. M., Freidinger, R. M., Pawluczyk, J. M., Perlow, D. S., Pettibone, D. J., and Veber, D. F. (1994) 1-((7,7-Dimethyl-2(S)-(2(S)-amino-4-(methylsulfonyl)butyramido)bicyclo [2.2.1]-heptan-1(S)-yl)methyl)sulfonyl)-4-(2-methylphenyl)piperazine (L-368,899): An orally bioavailable, non-peptide oxytocin antagonist with potential utility for managing preterm labor, *J. Med. Chem. 37*, 565−571.
30. Goodwin, T. M., Valenzuela, G. J., Silver, H., and Creasy, G. (1996) Dose ranging study of the oxytocin antagonist atosiban in the treatment of preterm labor. Atosiban Study Group, *Obstet. Gynecol. 88*, 331−336.
31. Schwarz, M. K., and Page, P. (2003) Preterm labour: An overview of current and emerging therapeutics, *Curr. Med. Chem. 10*, 1441−1468.
32. Cirillo, R., Gillio, T. E., Schwarz, M. K., Quattropani, A., Scheer, A., Missotten, M., Dorbais, J., Nichols, A., Borrelli, F., Giachetti, C., Golzio, L., Marinelli, P., Thomas, R. J., Chevillard, C., Laurent, F., Portet, K., Barberis, C., and Chollet, A. (2003) Pharmacology of (2S,4Z)-N-[(2S)-2-hydroxy-2-phenylethyl]-4-(methoxyimino)-1-[(2′-methyl[1,1′-biphenyl]-4-yl)carbonyl]-2-pyrrolidinecarboxamide, a new potent and selective nonpeptide antagonist of the oxytocin receptor, *J. Pharm. Exp. Ther. 306*, 253−261.
33. Strakova, Z., Copland, J. A., Lolait, S. J., and Soloff, M. S. (1998) ERK2 mediates oxytocin-stimulated PGE2 synthesis, *Am. Physiol. Soc. 274*, E634−E641.
34. Hoare, S., Copland, J. A., Strakova, Z., Ives, K., Jeng, Y. J., Hellmich, M. R., and Soloff, M. S. (1999) The proximal portion of the COOH terminus of the oxytocin receptor is required for coupling to g_q, but not g_i. Independent mechanisms for elevating intracellular calcium concentrations from intracellular stores, *J. Biol. Chem. 40*, 28682−28689.
35. Burns, P. D., Mendes, J. O. B., Jr., Yemm, R. S., Clay, C. M., Nelson, S. E., Hayes, S. H., and Silva, W. J. (2001) Cellular mechanisms by which oxytocin mediates ovine endometrial prostaglandin F2α synthesis: Role of G_i proteins and mitogen-activated protein kinases, *Biol. Reprod. 65*, 1150−1155.
36. Qian, A., Wang, W., and Sanborn, B. M. (1998) Evidence for the involvement of several intracellular domains in the coupling of oxytocin receptor to G $\alpha_{q/11}$, *Cell. Signalling 10*, 101−105.
37. Ballesteros, J. A., and Weinstein, H. (1995) Integrated methods for the construction of three-dimensional models and computational probing of structure−function relations in G protein-coupled receptors, *Methods Neurosci. 25*, 366−428.
38. Yang, M., Wang, W., Zhong, M., Phillipi, A., Lichtarge, O., and Sanborn, B. M. (2002) Lysine 270 in the third intracellular domain of the oxytocin receptor is an important determinant for Gα_q coupling specificity, *Mol. Endocrinol. 16*, 814−823.
39. Cheng, Y.-C., and Prusoff, W. H. (1973) Relationship between the inhibition constant (K1) and the concentration of inhibitor

which causes 50% inhibition (I50) of an enzymatic reaction, *Biochem. Pharmacol. 22*, 3099−3108.
40. Sali, A., and Blundell, T. L. (1993) Comparative protein modelling by satisfaction of spatial restraints, *J. Mol. Biol. 234*, 779−815.
41. Palczewski, K., Kumasaka, T., Hori, T., Behnke, C. A., Motoshima, H., Fox, B. A., Le Trong, I., Teller, D. C., Okada, T., Stenkamp, R. E., Yamamoto, M., and Miyano, M. (2000) Crystal structure of rhodopsin: A G protein-coupled receptor, *Science 289*, 739−745.
42. Brooks, B. R., Bruccoleri, R. E., Olafson, B. D., States, D. J., Swaminathan, S., and Karplus, M. (1983) Charmm: A program for macromolecular energy, minimization and dynamics calculations, *J. Comput. Chem. 4*, 187−217.
43. Farrens, D. L., Altenbach, C., Yang, K., Hubbell, W. L., and Khorana, H. G. (1996) Requirement of rigid-body motion of transmembrane helices for light activation of rhodopsin, *Science 274*, 768−770.
44. Rose, J. P., Wu, C. K., Hsiao, C. D., Breslow, E., and Wang, B. C. (1996) Crystal structure of the meurophysin-oxytocin complex, *Nat. Struct. Biol. 3*, 163−169.
45. Breton, C., Chellil, H., Kabbaj-Benmansour, M., Carnazzi, E., Seyer, R., Phalipou, S., Morin, M., Durroux, T., Zingg, H., Barberis, C., and Mouillac, B. (2001) Direct identification of human oxytocin receptor-binding domains using a photoactivatable cyclic peptide antagonist: Comparison with the human V1a vasopressin receptor, *J. Biol. Chem. 276*, 26931−26941.
46. Chini, B., Mouillac, B., Balestre, M.-N., Trumpp-Kallmeyer, S., Hoflack, J., Hibert, M., Andriolo, M., Pupier, S., Jard, S., and Barberis, C. (1996) Two aromatic residues regulate the response of the human oxytocin receptor to the partial agonist arginine vasopressin, *FEBS Lett. 397*, 201−206.
47. Hawtin, S. R., Howard, H. C., and Wheatley, M. (2001) Identification of an extracellular segment of the oxytocin receptor providing agonist-specific binding epitopes, *Biochem. J. 354*, 465−472.
48. Wesley, V. J., Hawtin, S. R., Howard, H. C., and Wheatley, M. (2002) Agonist-specific, high-affinity binding epitopes are contributed by an arginine in the N-terminus of the human oxytocin receptor. *Biochemistry 41*, 5086−5092.
49. Berde, B., and Boissonnas, R. A. (1968) in *Handbook of Experimental Pharmacology* (Berde, B., Ed.) Vol. 23, pp 802−870, Springer-Verlag, Berlin.
50. Chen, S., Xu, M., Lin, F., Lee, D., Riek, P., and Graham, R. M. (1999) Phe310 in transmembrane VI of the α1B-adrenergic receptor is a key switch residue involved in activation and catecholamine ring aromatic bonding, *J. Biol. Chem. 274*, 16320−16330.
51. Lazaridis, T. (2003) Effective energy function for proteins in lipid membranes, *Proteins: Struct., Funct., Genet. 52*, 176−191.
52. Themmen, A. P. N., and Huhtaniemi, I. (2000) Mutations of gonadotropins and gonadotropin receptors: Elucidating the physiology and pathophysiology of pituitary−gonadal function, *Endocr. Rev. 21*, 551−583.
53. Ascoli, M., Fanelli, F., and Segaloff, D. L. (2002) The lutropin/choriogonadotropin receptor, a 2002 perspective, *Endocr. Rev. 23*, 141−174.
54. Greasley, P. J., Fanelli, F., Scheer, A., Abuin, L., Nenniger-Tosato, M., De Benedetti, P. G., and Cotecchia, S. (2001) Mutational and computational analysis of the α1b-adrenergic receptor: Involvement of basic and hydrophobic residues in receptor activation and G protein coupling, *J. Biol. Chem. 276*, 46485−46494.
55. Ballesteros, J. A., Jensen, A. D., Liapakis, G., Rasmussen, S. G., Shi, L., Gether, U., and Javitch, J. A. (2001) Activation of the β_2-adrenergic receptor involves disruption of an ionic lock between the cytoplasmic ends of transmembrane segments 3 and 6, *J. Biol. Chem. 276*, 29171−29177.
56. Greasley, P. J., Fanelli, F., Rossier, O., Abuin, L., and Cotecchia, S. (2002) Mutagenesis and modelling of the α_{1b}-adrenergic receptor highlight the role of helix3/helix 6 interface in receptor activation, *Mol. Pharmacol. 61*, 1−8.
57. Shapiro, D. A., Kristiansen, K., Weiner, D. M., Kroeze, W. K., and Roth, B. L. (2002) Evidence for a model of agonist induced activation of 5-hydroxytryptamine 2A serotonin receptors that involves the disruption of a strong ionic interaction between helices 3 and 6, *J. Biol. Chem. 277*, 11441−11449.
58. Kjelsberg, M. A., Cotecchia, S., Ostrowski, J., Caron, M. G., and Lefkowitz, R. J. (1992) Constitutive activation of the α_{1B}-adrenergic receptor by all amino acid substitutions at a single site, *J. Biol. Chem. 267*, 1430−1433.
59. Seeber, M., De Benedetti, P. G., and Fanelli, F. (2003) Molecular dynamics simulations of the ligand-induced chemical information transfer in the 5-HT_{1A} receptor, *J. Chem. Inf. Comput. Sci. 43*, 1520−1531.
60. Vitale, R. M. C., Pedone, P., De Benedetti, P. G., and Fanelli, F. (2004) Structural features of the inactive and active states of the melanin-concentrating hormone receptors: Insights from molecular simulations, *Proteins: Struct., Funct., Bioinf. 56*, 430−448.
61. Fanelli, F. (2000) Theoretical study on mutation-induced activation of the luteinizing hormone receptor, *J. Mol. Biol. 296*, 1333−1351.
62. Angelova, K., Fanelli, F., and Puett, D. (2002) Engineered and simulated mutations in transmembrane helices 6 and 7 of the lutropin receptor: A model for constitutive and ligand-mediated receptor activation, *J. Biol. Chem. 277*, 32202−32213.
63. Okada, T., Fujiyoshi, Y., Silow, M., Navarro, J., Landau, E. M., and Shichida, Y. (2002) Functional role of internal water molecules in rhodopsin revealed by X-ray crystallography, *Proc. Natl. Acad. Sci. U.S.A. 99*, 5982−5987.
64. Gudermann, T., Schoneberg, T., and Schultz, G. (1997) Functional and structural complexity of signal transduction via G-protein-coupled receptors, *Annu. Rev. Neurosci. 20*, 399−427.
65. Parnot, C., Miserey-Lenkei, S., Bardin, S., Corvol, P., and Clauser, E. (2002) Lessons from constitutively active mutants of G protein-coupled receptors, *Trends Endocrinol. Metab. 13*, 336−343.
66. Cotecchia, S., Fanelli, F., Scheer, A., and De Benedetti, P. G. (1999) Constitutively active receptor mutants as probes for studying the mechanisms underlying G protein-coupled receptor activation, in *Receptor Biochemistry and Methodology* (Strader, C., and Sibley, D., Eds.) Vol. III, Structure/function analysis of GPCRs (Wess, J., Ed.), pp 167−183.
67. Cotecchia, S., Kobilka, B. K., Daniel, K. W., Nolan, R. D., Lapetina, E. Y., Caron, M. G., Lefkowitz, R. J., and Regan, J. W. (1990) Multiple second messenger pathways of α-adrenergic receptor subtypes expressed in eukaryotic cells, *J. Biol. Chem. 265*, 63−69.
68. Samama, P., Cotecchia, S., Costa, T., and Lefkowitz, R. J. (1993) A mutation-induced activated state of the β_2-adrenergic receptor. Extending the ternary complex model, *J. Biol. Chem. 268*, 4625−4636.
69. Bond, R. A., Leff, P., Johnson, T. D., Milano, C. A., Rockman, H. A., McMinn, T. R., Apparsundaram, S., Hyek, M. F., Kenakin, T. P., Allen, L. F., and Lefkowitz, R. J. (1995) Physiological effects of inverse agonists in transgenic mice with myocardial overexpression of the β2-adrenoceptor, *Nature 374*, 272−276.
70. Leff, P. (1995) The two-state model of receptor activation, *Trends Pharmacol. Sci. 16*, 89−97.
71. Perez, D. M., Hwa, J., Gaivin, R., Mathur, M., Brown, F., and Graham, R. M. (1996) Constitutive activation of a single effector pathway: Evidence for multiple activation states of a G protein-coupled receptor, *Mol. Pharmacol. 49*, 112−122.
72. Wiens, B. L., Nelson, C. S., and Neve, K. A. (1998) Contribution of serine residues to constitutive and agonist-induced signaling via the D2S dopamine receptor: Evidence for multiple, agonist-specific active conformations, *Mol. Pharmacol. 54*, 435−444.
73. Krumins, A. M., and Barber, R. (1997) The stability of the agonist β2-adrenergic receptor-Gs complex: Evidence for agonist-specific states, *Mol. Pharmacol. 52*, 144−154.
74. Scaramellini, C., and Leff, P. (1998) A three-state receptor model: Predictions of multiple agonist pharmacology for the same receptor type, *Ann. N.Y. Acad. Sci. 861*, 97−103.
75. Mhaouty-Kodja, S., Barak, L. S., Scheer, A., Abuin, L., Diviani, D., Caron, M. G., and Cotecchia, S. (1999) Constitutively active α-1b adrenergic receptor mutants display different phosphorylation and internalization features, *Mol. Pharmacol. 55*, 339−347.
76. Feng, Y. H., Miura, S., Husain, A., and Karnik, S. S. (1998) Mechanism of constitutive activation of the AT1 receptor: Influence of the size of the agonist switch binding residue Asn-(111), *Biochemistry 37*, 15791−15798.
77. Gilchrist, R. L., Ryu, K.-S., Ji, I., and Ji, T. H. (1996) The luteinizing hormone/chorionic gonadotropin receptor has distinct transmembrane conductors for cAMP and inositol phosphate signals, *J. Biol. Chem. 271*, 19283−19287.
78. Gether, U., Ballesteros, J. A., Seifert, R., Sanders-Bush, E., Weinstein, H., and Kobilka, B. K. (1997) Structural instability of a constitutively active G protein-coupled receptor. Agonist-independent activation due to conformational flexibility, *J. Biol. Chem. 272*, 2587−2590.

79. Samama, P., Bond, R. A., Rockman, H. A., Milano, C. A., and Lefkowitz, R. J. (1997) Ligand-induced overexpression of a constitutively active β2-adrenergic receptor: Pharmacological creation of a phenotype in transgenic mice, *Proc. Natl. Acad. Sci. U.S.A. 94*, 137−141.
80. Alewijnse, A. E., Smit, M. J., Hoffmann, M., Verzijl, D., Timmerman, H., and Leurs, R. (1998) Constitutive activity and structural instability of the wild-type human H2 receptor, *J. Neurochem. 71*, 799−807.
81. Rosenthal, W., Antaramian, A., Gilbert, S., and Birnbaumer, M. (1993) Nephrogenic diabetes insipidus. A V2 vasopressin receptor unable to stimulate adenylyl cyclase, *J. Biol. Chem. 368*, 13030−13033.
82. Acharya, S., and Karnik, S. S. (1996) Modulation of GDP release from transducin by the conserved Glu134-Arg135 sequence in rhodopsin, *J. Biol. Chem. 271*, 25406−25411.
83. Arora, K. K., Cheng, Z., and Catt, K. J. (1997) Mutations of the conserved DRS motif in the second intracellular loop of the gonadotropin-releasing hormone receptor affect expression, activation, and internalization, *Mol. Endocrinol. 11*, 1203−1212.
84. Chung, D. A., Wade, S. M., Fowler, C. B., Woods, D. D., Abada, P. B., Mosberg, H. I., and Neubig, R. R. (2002) Mutagenesis and peptide analysis of the DRY motif in the α2A adrenergic receptor: Evidence for alternate mechanisms in G protein-coupled receptors, *Biochem. Biophys. Res. Commun. 293*, 1233−1241.
85. Eason, M. G., Jacinto, M. T., and Liggett, S. B. (1994) Contribution of ligand structure to activation of α2-adrenergic receptor subtype coupling to Gs, *Mol. Pharmacol. 45*, 696−702.
86. Niedernberg, A., Blaukat, A., Schoneberg, T., and Kostenis, E. (2003) Regulated and constitutive activation of specific signalling pathways by the human S1P5 receptor, *Br. J. Pharmacol. 138*, 481−493.
87. Min, K.-S., Liu, X., Fabritz, J., Jaquette, J., Abell, A. N., and Ascoli, M. (1998) Mutations that induce constitutive activation and mutations that impair signal transduction modulate the basal and/or agonist-stimulated internalization of the Lutropin/Choriogonadotropin receptor, *J. Biol. Chem. 273*, 34911−34919.
88. Shinozaki, H., Fanelli, F., Liu, X., Jaquette, J., Nakamura, K., and Segaloff, D. L. (2001) Pleiotropic effects of substitutions of a highly conserved leucine in transmembrane helix III of the human lutropin/choriogonadotropin receptor with respect to constitutive activation and hormone responsiveness, *Mol. Endocrinol. 15*, 972−984.
89. Barroso, S., Richard, F., Nicolas-Ethève, D., Kitabgi, P., and Labbé-Jullié, C. (2002) Constitutive activation of the neurotensin receptor 1 by mutation of Phe(358) in Helix seven, *Br. J. Pharmacol. 135*, 997−1002.
90. Ballesteros, J., Kitanovic, S., Guarnieri, F., Davies, P., Fromme, B. J., Konvicka, K., Chi, L., Millar, R. P., Davidson, J. S., Weinstein, H., and Sealfon, S. C. (1998) Functional microdomains in G-protein-coupled receptors. The conserved arginine-cage motif in the gonadotropin-releasing hormone receptor, *J. Biol. Chem. 273*, 10445−10453.
91. Visiers, I., Ebersole, B. J., Dracheva, S., Ballesteros, J., Sealfon, S. C., and Weinstein, H. (2002) Structural motifs as functional microdomains in G protein coupled receptors: Energetic considerations in the mechanism of activation of the serotonin $5HT_{2A}$ receptor by disruption of the ionic lock of the arginine cage, *Int. J. Quantum Chem. 88*, 65−75.
92. Huang, P., Li, J., Chen, C., Visiers, I., Weinstein, H., and Liu-Chen, L.-Y. (2001) Functional role of a conserved motif in TM6 of the rat mu opioid receptor: Constitutively active and inactive receptors result from substitutions of Thr6.34(279) with Lys and Asp, *Biochemistry 40*, 13501−13509.
93. Fritze, O., Filipek, S., Kuksa, V., Palczewski, K., Hofmann, K. P., and Ernst, O. P. (2003) Role of the conserved NPxxY(x)5,6F motif in the rhodopsin ground state and during activation, *Proc. Natl. Acad. Sci. U.S.A. 100*, 2290−2295.
94. Wong, S. K. (2003) G protein selectivity is regulated by multiple intracellular regions of GPCRs, *Neurosignals 12*, 1−12.
95. López-Giménez, J. F., Villazón, M., Brea, J., Loza, M. I., Palacios, J. M., Mengod, G., and Vilaró, M. T. (2001) Multiple conformations of native and recombinant human 5-hydroxytryptamine(2a) receptors are labeled by agonists and discriminated by antagonists, *Mol. Pharmacol. 60*, 690−699.
96. Kenakin, T. (1995) Agonist-receptor efficacy. II. Agonist trafficking of receptor signals, *Trends Pharmacol. Sci. 16*, 188−192.
97. Kenakin, T. (1995) Agonist-receptor efficacy. I: Mechanisms of efficacy and receptor promiscuity, *Trends Pharmacol. Sci. 16*, 232−238.
98. Thibonnier, M., Preston, J. A., Dublin, N., Wilkins, P. L., Berti-Mattera, L. N., and Mattera, R. (1997) The human V3 pituitary vasopressin receptor: Ligand binding profile and density-dependent signaling pathways, *Endocrinology 138*, 4109−4122.
99. Weiss, J. M., Morgan, P. H., Lutz, M. W., and Kenakin, T. P. (1996) The cubic ternary complex receptor-occupancy model. III. resurrecting efficacy, *J. Theor. Biol. 181*, 381−397.
100. Terrillon, S., and Bouvier, M. (2004) Roles of G-protein-coupled receptor dimerization, *EMBO Rep. 5*, 30−34.
101. Agnati, L. F., Fuxe, K., and Ferrè, S. H. (2005) How receptor mosaics decode transmitter signals. Possible relevance of cooperativity. *Trends Biochem. Sci. 30*, 188−193.

BI0509853